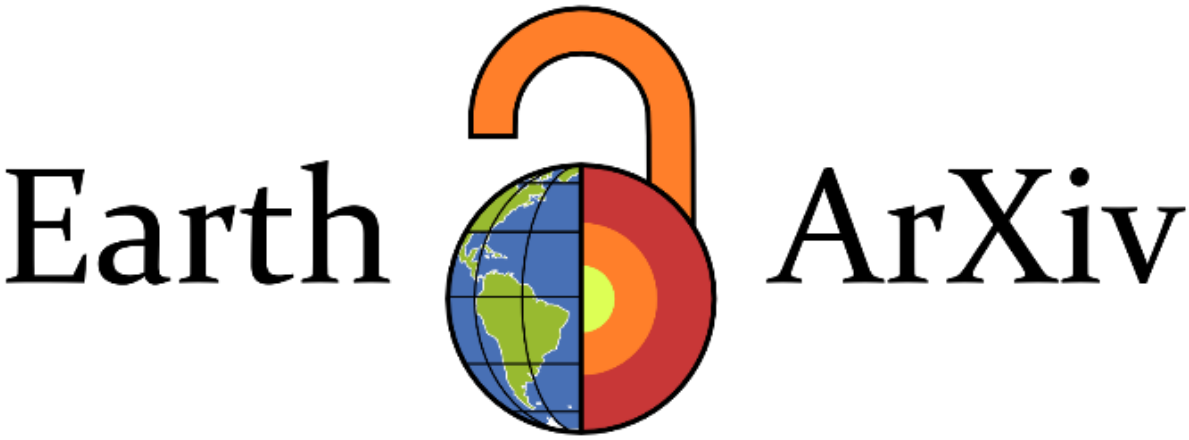

From buffer-based tables to dynamic response curves for soil-specific lime requirement estimation using machine learning

Hamza Jouichat [a,1], Lotfi Khiari [a,*,2]

[a]Department of Soil Science and Agrifood Engineering, Laval University, Québec, QC, Canada
[1] ORCID: 0000-0003-4957-2854.
[2] ORCID: 0000-0003-3793-1186.
* Corresponding author: lotfi.khiari@fsaa.ulaval.ca

ABSTRACT

Accurate estimation of lime requirement (LR) remains a major challenge in acid soils, as conventional buffer-based approaches, particularly the Shoemaker–McLean–Pratt (SMP) method, rely on a single equilibrium measurement and predefined target pH values, limiting their ability to capture the diversity of soil neutralization responses. This study evaluated whether machine-learning (ML) models can reconstruct incubation-derived neutralization curves and provide flexible, soil-specific LR estimates without reliance on SMP buffer chemistry. A total of 400 soil samples from Eastern North America were incubated at six $CaCO_3$ application rates. Soil responses were expressed as pH change (ΔpH) and fitted using a Mitscherlich model to derive reference neutralization curves and incubation-based LR. ML models were developed using four predictor classes: mid-infrared (MIR) spectroscopy, visible–near infrared (VisNIR) spectroscopy, routine chemistry (RC), and detailed pedological characterization (DPC), as well as hybrid combinations. ΔpH predictions were robust across all models, with DPC achieving the highest performance (R^2 = 0.92, RMSE = 0.24 pH units under cross-validation), followed by RC and MIR, while VisNIR and minimal SMP-based models showed lower accuracy. LR estimates derived from reconstructed ML curves consistently exhibited lower prediction errors than regional SMP-based recommendations across all target pH levels. Notably, inclusion of SMP buffer pH did not improve model performance when broader chemical or spectral descriptors were available. These results demonstrate that curve-based ML approaches provide a viable alternative to equilibrium-based buffer methods by enabling continuous, soil-specific representation of liming response. This framework supports a transition from static recommendation systems to dynamic, data-driven strategies, laying the foundation for precision liming.

Keywords: Soil acidity; Liming; Buffer capacity; Mitscherlich model; soil spectroscopy; Precision agriculture

1. Introduction

Soil acidity remains a major constraint to crop production in temperate regions, as it reduces nutrient availability, restricts root growth, and increases the solubility of toxic elements such as aluminum (Fageria and Baligar, 2008; Goulding, 2016). Soil pH is therefore a key integrator of soil chemical functioning, controlling base cation availability, aluminum toxicity, and long-term soil fertility (Sumner and Noble, 2003; von Uexküll and Mutert, 1995). Under these conditions, liming remains the primary management practice for ameliorating acid soils. Its effectiveness, however, depends critically on the accurate estimation of LR, defined as the amount of calcium carbonate needed to raise soil pH to a target value suitable for crop production (Shoemaker et al., 1961; Adams, 1984; Tran and Van Lierop, 1982). Because LR depends not only on initial pH but also on soil buffering capacity, exchange processes, and organo-mineral interactions, inaccurate estimation may lead to both under-liming and over-liming, with agronomic and economic consequences (Thomas and Hargrove, 1984; Sumner and Noble, 2003; Fageria and Baligar, 2008).

Soil–lime incubation is widely regarded as the agronomic reference for LR calibration, as it directly captures the soil pH response to increasing lime additions while allowing time for equilibration between the soil and the amendment (Woodruff, 1948; Adams, 1984; Liu et al., 2004; Godsey et al., 2007). However, incubation is impractical for routine laboratory use due to its high cost, long equilibration times, and intensive sample-handling requirements (Alley and Zelazny, 1987; Kissel et al., 2007). To overcome these limitations, buffer-based methods were developed to infer LR from a single equilibrium measurement (Van Lierop, 1990). Among them, the Shoemaker–McLean–Pratt (SMP) buffer method became the dominant operational approach in North America, enabling rapid conversion of buffer pH into lime recommendations using regional calibration tables (Shoemaker et al., 1961; Follett and Follett, 1983; Van Lierop and Tran, 1983). Despite their operational simplicity, SMP-based systems exhibit both structural and conceptual limitations. Their calibration relies on empirical relationships derived from relatively small and region-specific datasets, which may not adequately represent broader pedological variability (McLean et al., 1978; Tran and Van Lierop, 1982). More fundamentally, by condensing soil neutralization demand into a single buffer pH value, these approaches reduce a continuous, soil-specific process to a single scalar descriptor. This simplification cannot explicitly account for the combined effects of exchangeable acidity, pH-dependent charge, aluminum hydrolysis, and mineral–organic interactions that govern soil buffering

behavior. As a result, lime recommendations can be highly sensitive to small analytical deviations; for example, differences of ±0.2 pH units in SMP measurements may translate into uncertainties of approximately ±2–3 t ha^{-1} in LR for Québec soils (Lemire et al., 2006). In addition, these systems typically provide recommendations for only a limited number of predefined target pH values, leaving little flexibility to adjust liming decisions to crop requirements, economic conditions, or site-specific constraints. Similar concerns have been raised in other regions. In France, COMIFER (2009) revised its LR recommendation framework to place greater emphasis on cation exchange capacity (CEC) and base saturation, partly in response to the observed variability of soil pH measurements across sampling periods. This shift illustrates the need to rely on more stable pedological descriptors when pH-based indicators alone do not provide sufficiently robust guidance. The case for alternatives is further strengthened by the use of SMP buffer solutions involving reagents associated with recognized environmental and health concerns (IARC, 2012; NIOSH, 2013; Sikora, 2006; Wolf et al., 2008). These limitations point to the need for a different conceptual framework for lime recommendation. Rather than predicting a single lime rate linked to a limited set of fixed pH targets, a more flexible approach is to model the soil neutralization response itself. This involves reconstructing the relationship between pH change and increasing $CaCO_3$ application rates, and then deriving LR for any user-defined target pH. Such a framework replaces static, table-based recommendations with a continuous, soil-specific description of neutralization behavior, more closely aligned with how liming decisions are made in practice. This concept was first demonstrated by Jouichat and Khiari (2026), who showed that complete neutralization curves could be reconstructed from titration data using machine-learning models based on chemical and spectral predictors. That work established a key proof of concept: soil buffering behavior can be inferred from high-dimensional soil information rather than approximated through a single buffer measurement. However, titration reflects short-term chemical equilibria and does not fully capture the kinetics of neutralization observed under incubation conditions. Because incubation has historically underpinned agronomic LR calibration, extending dynamic modeling beyond titration to incubation represents a critical, more relevant step.

The present study was designed to address this challenge. It extends dynamic, machine-learning-based reconstruction from titration-derived to incubation-derived neutralization curves, thereby targeting the experimental framework most directly linked to agronomic LR determination. Using a large dataset of soils

spanning a wide pedological gradient across Eastern North America, this study provides a robust basis for reassessing conventional LR estimation approaches and developing more generalizable alternatives. In addition, it evaluates multiple predictor families that differ in analytical cost and operational requirements, including RC, DPC, VisNIR spectroscopy, and MIR spectroscopy. Together, these approaches define a flexible, multi-level prediction framework adaptable to diverse laboratory contexts.

The objective of this study was therefore to determine whether machine-learning models can reconstruct incubation-derived neutralization curves and provide flexible, soil-specific LR estimates across a wide diversity of acid soils. Specifically, we (i) evaluated the ability of different predictor families to predict soil pH change and reconstruct neutralization curves, (ii) assessed their performance for estimating LR across target pH values, and (iii) examined their potential to support a transition from static, buffer-based recommendation systems toward dynamic, response-based approaches for precision liming.

2. Materials and methods

2.1. Soil sampling and routine analysis

A total of 400 soils were included in this study, covering a broad pedological gradient across eastern North America. The dataset comprised 363 soils from Québec, 7 from Ontario, 15 from Prince Edward Island, and 15 from the state of Maine, USA (Fig. 1). After collection, all samples were air-dried under laboratory conditions and gently crushed to pass a 2 mm sieve before analysis. This soil collection overlaps substantially with that used in Jouichat and Khiari (2026). Still, the present study extends the analytical description to support incubation-based modeling and to evaluate multiple predictor families.

To support the RC approach, water pH was measured at a 1:1 soil-to-solution ratio (v/v). SMP buffer pH was determined by adding a volume of SMP buffer equal to that of the soil–water suspension before pH measurement (CEAEQ, 2014; Shoemaker et al., 1961). Soil organic matter (SOM) was determined using the Walkley–Black procedure (Nelson and Sommers, 1982; Walkley and Black, 1934). Mehlich-3 extraction (Mehlich, 1984) was used to quantify a range of extractable major and trace elements, which were subsequently measured by inductively coupled plasma spectrometry (Thermo Jarrell-Ash model 61-E, Thermo Instrument, Franklin, MA).

To support the DPC approach, particle-size distribution was determined following the method of Day (1965), from which sand, silt, and clay contents were obtained. CEC, exchangeable base cations ($Ca^{2}_{(NH_4OAc)}$, $Mg^{2+}_{(NH_4OAc)}$, $K^{+}_{(NH_4OAc)}$, and $Na^{+}_{(NH_4OAc)}$), and base saturation were determined using ammonium acetate extraction at pH 7 method according to Lavkulich (1981) and CPVQ (1997). Mehlich-3 extractable Al (Al_{M3}) was considered part of the routine chemical signature, whereas ammonium acetate extractable Al was quantified together with exchangeable base cations during the CEC procedure; however, exchangeable acidity-related Al was represented by the KCl-extractable fraction. Exchangeable acidity ($H^+ + Al^{3+}$) was measured by potassium chloride extraction and titration, as described by Thomas (1982).

Descriptive statistics for all variables used in the RC and DPC predictor sets are presented in Table 1.

Table 1
Descriptive statistics of selected routine-chemistry and detailed pedological properties of 400 soils from Eastern North America.

Soil property	Mean	SD	Min	$Q1_{25th\ Percentile}$	$Q2_{50th\ Percentile}$	$Q3_{75th\ Percentile}$	Max	Skewness	Kurtosis
Routine chemistry (RC):									
pH_{water}	5.67	0.60	4.05	5.24	5.71	6.12	6.89	-0.26	-0.43
pH_{SMP}	6.46	0.41	4.63	6.28	6.49	6.74	7.33	-1.17	2.50
	---------- g kg^{-1}----------								
SOM	51.7	36.4	0.5	31.3	42.6	59.2	296.6	3.03	13.15
	---------- mg kg^{-1}----------								
K_{M3}	124	127	7	52	88	148	1163	3.71	21.05
Ca_{M3}	1472	1049	45	743	1294	1950	6399	1.48	3.33
Mg_{M3}	172	158	6	63	119	219	901	1.67	2.64
Na_{M3}	31	21	0	16	30	42	158	1.70	6.32
B_{M3}	55	223	0	3	3	6	1228	4.31	17
Cu_{M3}	1.85	1.74	0.00	0.89	1.54	2.24	18.02	3.75	23.93
Mn_{M3}	40.11	55.95	0.65	9.47	21.57	44.11	406.84	3.15	11.81
Zn_{M3}	5.67	10.08	0.16	1.63	2.77	5.06	79.98	4.35	21.12
Mo_{M3}	0.07	0.32	0.00	0.00	0.00	0.01	2.98	5.66	35.31
Ni_{M3}	0.56	1.23	0.00	0.00	0.26	0.64	18.07	8.98	112.02

Cd_{M3}	0.07	0.06	0.00	0.04	0.06	0.08	0.55	3.00	14.29
Cr_{M3}	0.13	0.13	0.00	0.06	0.11	0.17	1.06	3.24	17.74
Co_{M3}	0.25	0.24	0.00	0.13	0.20	0.31	3.30	6.44	73.62
Pb_{M3}	1.50	1.32	0.00	0.79	1.23	1.83	12.42	3.54	20.65
	---------- mg L^{-1} ----------								
P_{M3}	61.45	64.84	1.94	20.03	37.30	77.20	401.00	2.18	5.42
Fe_{M3}	199.60	87.92	0.58	150.75	195.50	244.25	662.49	0.48	2.83
Al_{M3}	969.86	484.6	3.30	676.75	852.00	1265	2540	0.56	0.34
	Detailed pedological characterization (DPC)								
	---------- g kg^{-1} ----------								
Clay	134	118	0	60	93	159	633	1.80	2.78
Sand	511	209	67	355	526	670	969	-0.13	-0.75
Silt	355	150	4.8	240	349	451	754	0.21	-0.44
	---------- $cmol^{+}$ kg^{-1} ----------								
CEC	23.02	12.77	4.32	14.86	20.18	27.48	124.95	2.58	12.53
K_{NH_4OAc}	0.31	0.31	0.00	0.11	0.23	0.42	2.8	2.71	12.75
Ca_{NH_4OAc}	9.38	7.89	0.04	4.75	8.14	12.35	92.00	4.03	33.38
Mg_{NH_4OAc}	1.67	1.65	0.00	0.60	1.09	2.03	8.34	1.70	2.42
Na_{NH_4OAc}	0.31	3.22	0.05	0.04	0.08	0.17	63.21	19.38	375.88
Al_{NH_4OAc}	0.06	0.12	0.00	0.01	0.02	0.05	0.85	4.11	19.41
Exch. acidity	0.39	0.81	0	0.05	0.1	0.28	5.65	3.67	14.61
	---------- % ----------								
Base saturation	49	23	1	37	52	66	92	0.16	2.98

pH_{water}: soil pH measured in water; **pH_{SMP}**: SMP buffer pH: **SOM**: Soil organic matter; **M3**: Mehlich-3 extractable; **CEC**: cation exchange capacity; NH_4OAc: ammonium acetate (pH 7.0); **Exch. acidity**: exchangeable acidity (Al^{3+} + H^{+}); **SD**: standard deviation; **Min**: minimum; **Max**: maximum; **Q1**: first quartile (25th percentile); **Q2**: median (50th percentile); **Q3**: third quartile (75th percentile).

2.2. Soil–$CaCO_3$ incubation procedure

The incubation experiment was designed to generate soil-specific neutralization curves describing the long-term pH response of each soil to increasing $CaCO_3$ additions. For each soil, seven $CaCO_3$ rates (D_0–D_6) were applied,

including an untreated control and six increasing lime rates. The highest rate was selected to ensure that soil pH reached or exceeded neutrality. To account for differences in soil buffering capacity, the applied $CaCO_3$ rates were defined according to LR classes derived from the soil–$Ca(OH)_2$ titration procedure described by Jouichat and Khiari (2026). Table 2 summarizes the graduated $CaCO_3$ rates used for the different LR_{Tit} classes. Following dose selection, the required amount of laboratory-grade $CaCO_3$ was weighed with an analytical balance (±0.0001 g) and thoroughly dry-mixed with 200 g of soil. The amended samples were then incubated at controlled room temperature (21–25 °C) for 23 weeks. During incubation, water was added weekly to maintain soil moisture near field capacity, and the samples were periodically mixed to promote uniform lime–soil contact. At the end of the incubation period, soils were air-dried, and the final pH was measured in a 1:1 soil-to-water suspension. The resulting dataset was used to derive continuous pH-gain response curves rather than only endpoint LR values.

Table 2.
$CaCO_3$ application rate scheme used for soil incubation across LR_{Tit} classes.

LR_{Tit} (t ha^{-1})	D_0	D_1	D_2	D_3	D_4	D_5	D_6
< 4	0.0	0.25	0.50	1.00	2.00	3.00	6.00
4 – 8		0.50	1.00	2.00	4.00	6.00	10.00
8 – 12		1.00	3.00	6.00	9.00	12.00	16.00
12 – 16		1.50	3.00	6.00	9.00	15.00	20.00
16 – 20		3.00	6.00	9.00	12.00	18.00	26.00
> 20		4.00	8.00	12.00	20.00	28.00	40.00

$\boldsymbol{LR_{Tit}}$ denotes the lime requirement estimated from soil–$Ca(OH)_2$ titration, expressed as t ha^{-1} $CaCO_3$ equivalent, according to Jouichat and Khiari (2026); D_0 is the untreated control; *D1–D_6* represent the six $CaCO_3$ application rates used in the incubation experiment.

2.3. Spectral data acquisition

To characterize the soils, both MIR and VisNIR spectra were acquired. Spectral measurements followed the same general procedures as those used by Jouichat and Khiari (2026) to maintain analytical consistency between the titration- and incubation-based datasets.

2.3.1. Mid-infrared (MIR)

Air-dried soil samples were finely ground to pass a 0.2 mm sieve before MIR analysis. Spectra were collected in transmission mode with a Bruker TENSOR II spectrometer (Bruker Optics, Billerica, MA, USA), equipped with an HTS-XT module and an MCT detector. The spectral range extended from 599.79 to 3997.15 cm^{-1}, with a nominal data interval of 1.43 cm^{-1} and a spectral resolution of 4 cm^{-1}, as configured in OPUS. For each soil, four replicate measurements were obtained from four separate wells of a stainless-steel sample holder, and the averaged spectrum was retained for subsequent analyses. Before each measurement series, a reference spectrum was recorded from an empty well with an anodized aluminum base to account for instrumental drift and atmospheric contributions.

2.3.2. Visible–near infrared (VisNIR)

For VisNIR analysis, air-dried soil samples sieved to 2 mm were scanned in diffuse reflectance mode in a dark room using an ASD FieldSpec 4 spectroradiometer (Analytical Spectral Devices Inc., Boulder, CO, USA). Spectra were collected over the 350–2500 nm range at 1 nm intervals. The soil was placed in a glass vial, and reflectance was measured directly above the vial opening. A Spectralon white reference standard was scanned before each batch to correct for instrument drift and ambient light variation.

2.4. Modeling incubation-derived neutralization curves

To describe soil-specific neutralization responses under incubation, the observed pH values were first expressed as pH gain relative to the initial condition, rather than as absolute pH values. For a given soil, pH gain at lime rate x was defined as the difference between the equilibrium pH measured after incubation and the initial soil pH before $CaCO_3$ addition. Expressing the response in this way isolates the net effect of liming and facilitates

comparison among soils with differing initial pH values. The relationship between pH gain and increasing $CaCO_3$ rates was then described using a two-parameter Mitscherlich-type exponential model (Mitscherlich, 1909) (Eq. 1).

$$\boldsymbol{\Delta pH(x) = A\left(1 - e^{-k\,x}\right)} \quad (\mathbf{1})$$

Where ΔpH(x) is the predicted pH gain at lime rate x (t ha^{-1}), A is the asymptotic maximum pH gain, and $\boldsymbol{k}$ is a curvature parameter controlling how rapidly the response approaches its asymptote. Predicted absolute pH values were reconstructed by adding the initial soil pH, pH0 to the modeled pH gain (Eq. 2).

$$\boldsymbol{pH(x) = pH_0 + \Delta pH(x)}, \quad (\mathbf{2})$$

with pH_0 the initial soil pH.

Model parameters (A, k) were estimated for each soil by nonlinear least squares using the Levenberg–Marquardt algorithm (Levenberg, 1944; Marquardt, 1963). Initial values were set as $\boldsymbol{A_0 = pH_{max,obs} - pH_0}$, $\boldsymbol{k_0 = 0.1}$, with the constraints $\boldsymbol{A \geq 0}$ and $\boldsymbol{k > 0}$.

Once fitted, the model provided a continuous neutralization curve from which the lime requirement (LR_{Inc}) corresponding to any target pH (pH_{Target}) could be analytically derived. Solving Eq. (2) for x gives (Eq. 3).

$$\boldsymbol{LR_{Inc} = -\frac{1}{k}\ln\left(1 - \frac{pH_{Target} - pH_0}{A}\right)} \quad (\mathbf{3})$$

Where LR_{Inc} is the incubation-derived lime requirement, expressed as t ha-1 $CaCO_3$ equivalent. This formulation enables continuous estimation of lime requirement for any user-defined target pH, rather than restricting recommendations to a limited set of predefined thresholds.

2.5. Spectral preprocessing and feature engineering

Before model development, MIR and VisNIR spectra were standardized to reduce dimensionality, minimize edge-related noise, and improve compatibility across spectral datasets. MIR spectra were restricted to the 650–

3950 cm^{-1} range, whereas VisNIR spectra were restricted to 450–2450 nm. The trimmed spectra were then resampled to constant intervals of 10 cm^{-1} for MIR and 10 nm for VisNIR. This step removed spectral regions dominated by instrumental noise or atmospheric interference while reducing collinearity and computational burden without materially affecting the chemical information available for prediction. A preliminary exploratory evaluation showed that this reduced-resolution representation preserved predictive performance while substantially improving computational efficiency, and was therefore retained for all subsequent analyses. To account for variation in sample presentation and light-scattering effects, several spectral pretreatment strategies were then evaluated. The standard normal variate (SNV) was used to correct for multiplicative scatter associated with particle-size heterogeneity and packing differences (Barnes et al., 1989; Rinnan et al., 2009). Savitzky–Golay smoothing without differentiation (SG0) was used to attenuate high-frequency noise while preserving major absorption features, whereas the first-derivative form (SG1) was used to reduce baseline effects and enhance the resolution of overlapping peaks (Savitzky and Golay, 1964). Detrending (DT) was also tested after SNV to correct residual curvature in the spectral baseline using a second-order polynomial adjustment (Barnes et al., 1989; Rinnan et al., 2009). The different pretreatment combinations were assessed separately for MIR and VisNIR data through preliminary model calibration to identify the preprocessing pipeline yielding the best predictive performance in each spectral domain. Based on this procedure, SG1-SNV was retained for MIR spectra, whereas SG1 alone was retained for VisNIR spectra (Fig. 2).

2.6. Target variable and predictor sets

The reconstruction of incubation-derived soil neutralization curves was based on the prediction of pH gain in response to laboratory-grade $CaCO_3$ application. For each soil and each amendment rate, pH gain was defined (Eq. 4).

$$\boldsymbol{\Delta pH_i = pH_i - pH_0} \quad (\mathbf{4})$$

where $\boldsymbol{pH_i}$ is the equilibrium soil pH measured after the $\boldsymbol{i}^{\text{th}}$ $CaCO_3$ addition and $\boldsymbol{pH_0}$ is the initial soil pH measured before amendment. Expressing the response as pH gain rather than absolute pH allowed the models to focus on the net neutralization response of each soil independently of its initial pH level.

Three main classes of predictive models were evaluated to compare the respective and combined contributions of chemical and spectral information: chemical-only, spectral-only, and hybrid models. In all cases, cumulative $CaCO_3$ rate (t ha^{-1}) was included as an essential covariate because of its direct mechanistic relationship with soil neutralization response.

Within the chemical-only class, two nested predictor sets were defined. The RC set included only routine analytical variables. The DPC-based set extended RC by adding the detailed pedological characterization, namely cation exchange capacity, exchangeable bases, base saturation, exchangeable acidity, and particle-size fractions. To assess the dependence of model performance on the SMP buffer test, which remains the main operational method for LR estimation in the study region (Shoemaker et al., 1961; CEAEQ, 2014), both DPC and RC were further evaluated with and without SMP buffer pH. Two additional simplified chemical configurations were also tested: an SMP-only model, including SMP pH and $CaCO_3$ rate only, and a pH-pair model combining water pH, SMP pH, and $CaCO_3$ rate.

The spectral-only class relied exclusively on preprocessed spectral data, either MIR or VisNIR, together with $CaCO_3$ rate. These models were intended to assess the predictive potential of each spectral domain without support from wet-chemistry variables. The hybrid class combined one or both spectral domains with selected chemical predictor sets, including water pH alone, RC (with or without SMP), and DPC (with or without SMP). These combinations were designed to test whether spectral and chemical information provided complementary value for reconstructing incubation-derived neutralization curves, and to quantify the additional contribution of detailed pedological variables.

To identify the most informative predictors among the chemical variables, all DPC-, RC-, and hybrid-based chemical inputs were first screened for multicollinearity using pairwise Pearson correlations. For each pair of variables with $|\boldsymbol{r}| > \mathbf{0.75}$, one variable was removed before model fitting. The reduced chemical predictor set was then submitted to recursive feature elimination with cross-validation (RFECV) (Guyon et al., 2002). In this procedure, chemical predictors were evaluated sequentially based on their contribution to cross-validated model performance, whereas MIR and VisNIR data were treated as single blocks rather than individual wavelengths. This block-wise strategy avoided the computational burden associated with wavelength-by-wavelength

elimination, preserved the internal structure of spectral information, and restricted feature selection to the chemical domain. At each iteration, the subset of predictors yielding the highest mean validation R^2 was retained. Pure spectral models were not subjected to RFECV, and in hybrid models each spectral domain counted as a single feature block.

2.7. Model algorithms and evaluation strategy

2.7.1. Random forest

Random forests (Breiman, 2001) were used as a nonparametric ensemble learning method to model the relationship between predictor sets and soil pH gain. The method combines many regression trees, each fitted to a bootstrap sample of the training data, while introducing additional randomness by considering only a subset of predictors at each split. This dual randomization reduces variance, limits overfitting, and improves predictive robustness. For a given input vector $\mathbf{X}$, the random forest prediction is obtained by averaging the outputs of the individual trees (Eq. 5).

$$\hat{\boldsymbol{y}} = \frac{\mathbf{1}}{\boldsymbol{m}} \sum_{\boldsymbol{j=1}}^{\boldsymbol{m}} \boldsymbol{T_j}(\boldsymbol{X}) \,. \qquad (\mathbf{5})$$

where m is the number of trees in the ensemble, and $T_j(X)$ is the prediction produced by the j^{th} tree. The hyperparameters optimized for the random forest models included the number of trees, maximum tree depth, the number of predictors considered at each split, the minimum number of samples required to split an internal node, and the minimum number of samples required in terminal nodes.

2.7.2. Cubist

Cubist (Quinlan, 1992) was used as a rule-based regression algorithm to model complex relationships between the predictor sets and soil pH gain. The method partitions the predictor space into a series of regions defined by rule conditions and fits a multivariate linear regression model within each terminal region. In this way, Cubist combines the flexibility of tree-based partitioning with the local interpretability of linear models. To improve predictive stability, Cubist can aggregate several rule-based models, referred to as committees, and obtain the

final prediction by averaging their outputs. Additional refinement can be introduced through nearest-neighbor smoothing, in which the rule-based prediction is adjusted based on the observed responses of the most similar training samples. The hyperparameters optimized for Cubist included the number of committees, the maximum number of rules per committee, and the number of neighbors used for smoothing.

2.7.3. Model training, hyperparameter optimization, and evaluation

All models were trained and evaluated using a soil-level splitting strategy to ensure that observations from the same incubation curve were kept within the same subset. The dataset was first divided into 80% training soils and 20% hold-out soils. Hyperparameters were optimized within the training subset using Bayesian optimization implemented with Optuna (Akiba et al., 2019). A total of 100 optimization iterations were performed, and each candidate configuration was assessed by fivefold cross-validation using mean squared error as the optimization criterion. All models were implemented in Python 3.12 (Van Rossum and Drake, 2009). Random forest models were trained using scikit-learn 1.5 (Pedregosa et al., 2011), and Cubist models were fitted using the Cubist 0.1.3 package for Python (Quinlan, 1992). Random forest was used for all chemical-only model configurations, whereas Cubist was used for all spectral-only and hybrid model configurations. The optimal hyperparameter combination was then used to refit the final model on the complete 80 % training subset. Evaluation A consisted of applying the tuned model to the independent 20% hold-out subset. This evaluation provided a fully independent assessment of pointwise predictive performance after model selection and hyperparameter optimization. Evaluation B was designed to evaluate model performance across the full dataset while enabling reconstruction of all incubation curves. Using the hyperparameters selected during Evaluation A, a tenfold cross-validation was performed at the soil level on the entire dataset, such that all observations from a given soil were assigned to the same validation fold and each soil was predicted exactly once. This procedure enabled comparison of observed and predicted pH-gain profiles for each soil and the derivation of curve-level prediction errors, in addition to summary performance metrics. The overall workflow, from feature preprocessing and model fitting to the two-stage evaluation procedure, is summarized in Fig. 3.

2.8. Performance metrics

Model performance was assessed using complementary metrics describing prediction accuracy, explained variance, relative predictive ability, and systematic deviation between observed and predicted values. These metrics included the root mean squared error (RMSE), coefficient of determination (R^2), ratio of performance to interquartile distance (RPIQ), regression slope, regression intercept, and bias. RMSE was used to quantify the average magnitude of prediction errors (Eq. 6).

$$\mathrm{RMSE} = \sqrt{\frac{1}{N}\sum_{i=1}^{N}(y_i - \hat{y}_i)^2} \quad (6)$$

where y_i ands, $\hat{y}_i$ are the observed and predicted values, respectively, and *N* is the number of observations. Lower RMSE values indicate better predictive accuracy. The coefficient of determination was calculated as (Eq. 7).

$$R^2 = 1 - \frac{\sum_{i=1}^{N}(y_i - \hat{y}_i)^2}{\sum_{i=1}^{N}(y_i - \bar{y})^2} \quad (7)$$

where $\bar{y}$ is the mean of the observed values. Higher R^2 values indicate that the model explains a greater proportion of the observed data's variance. RPIQ was used to express predictive performance relative to the spread of the observed data: (Eq. 8).

$$\mathrm{RPIQ} = \frac{\mathrm{IQR}}{\mathrm{RMSE}} \quad (8)$$

where IQR is the interquartile range of the observed values. Higher RPIQ values indicate better predictive performance relative to data variability. To evaluate systematic agreement between predictions and observations, a simple regression of predicted values against observed values was also considered. The slope was calculated as (Eq. 9).

$$\mathrm{Slope} = \frac{\sum_{i=1}^{N}(y_i - \bar{y})(\hat{y}_i - \bar{\hat{y}})}{\sum_{i=1}^{N}(y_i - \bar{y})^2} \quad (9)$$

and the intercept as (Eq. 10):

$$\mathrm{Intercept} = \bar{\hat{y}} - \mathrm{Slope} \times \bar{y} \quad (10)$$

where $\bar{y}$ and $\bar{\hat{y}}$ are the means of observed and predicted values, respectively. A slope close to 1 and an intercept close to 0 indicate good agreement between predicted and observed values. Bias was calculated as (Eq. 11):

$$\boldsymbol{Bias} = \frac{\mathbf{1}}{\boldsymbol{N}}\sum_{\boldsymbol{i=1}}^{\boldsymbol{N}}(\hat{\boldsymbol{y}}_{\boldsymbol{i}} - \boldsymbol{y}_{\boldsymbol{i}}) \quad (\mathbf{11})$$

Bias values close to 0 indicate limited systematic over- or under-prediction.

For Evaluation A, all performance metrics were computed on the independent hold-out subset. For Evaluation B, the same metrics were calculated for each validation fold, and their mean across folds was used to summarize model consistency and generalization performance.

2.9. Permutation-based feature importance

Permutation importance was used to quantify each predictor's contribution to model performance by measuring the increase in prediction error caused by randomly shuffling its values, thereby disrupting its relationship with the response variable (Altmann et al., 2010). For each predictor and for each validation fold of Evaluation B, the predictor values were randomly permuted 30 times while all other inputs were left unchanged. After each permutation, the root mean squared error (RMSE) was recalculated, and the corresponding increase in error relative to the unpermuted model was recorded as ΔRMSE. The importance score of a given predictor was then computed as the mean ΔRMSE, first averaged across the 30 permutations within each fold and then across all folds. Predictors associated with larger increases in RMSE were interpreted as making a stronger contribution to model performance.

2.10 Comparison with regional SMP-based recommendation protocols

To benchmark the proposed machine-learning and incubation-derived LR estimates against current regional practices, we applied the SMP-buffer recommendation tables used in Québec and Ontario. Québec recommendations were taken from the Centre de référence en agriculture et agroalimentaire du Québec (CRAAQ, 2010), whereas Ontario recommendations were taken from Munroe et al. (2018). In both cases, the tables provide $CaCO_3$ rates (t ha^{-1}) required to raise soil pH to predefined target values based on measured SMP buffer pH. For

each soil, the measured SMP buffer pH was matched to the closest tabulated buffer class in each provincial guide, and the corresponding recommended $CaCO_3$ rate was extracted. The Québec guide recommends target pH values of 5.5, 6.0, and 6.5, whereas the Ontario guide includes an additional target pH of 7.0. These SMP-based recommendations were compared with two alternative sources of LR:

- Incubation-derived lime requirements ($\boldsymbol{LR_{Inc}}$), calculated analytically from Mitscherlich-fitted neutralization curves (Eq. 3);
- Machine-learning–predicted lime requirements ($\boldsymbol{LR_{pred}}$) obtained in three steps. First, predicted pH gain values ($\widehat{\boldsymbol{\Delta pH_x}}$) at each of the six nonzero $CaCO_3$ rate were added to the soil's initial pH ($\boldsymbol{pH_0}$) reconstruct the predicted pH-rate curve (Eq. 12):

$$\widehat{\boldsymbol{pH}}_{\boldsymbol{x}} = \boldsymbol{pH_0} + \widehat{\boldsymbol{\Delta pH}}_{\boldsymbol{x}}, \qquad (\mathbf{12})$$

reconstruct the predicted pH-rate curve $(\boldsymbol{x}, \widehat{\boldsymbol{pH}}_{\boldsymbol{x}})$ was fitted to the Mitscherlich model (Eq. 1) to re-estimate the asymptote $\boldsymbol{A}$ and curvature parameter $\boldsymbol{k}$. Third, for each agronomic target pH $(\boldsymbol{pH}_{\text{target}})$ the corresponding LR_{pred} was obtained by inverting the fitted model as described in Eq. (3).

Finally, SMP-based recommendations were compared against the incubation-derived reference LR_{Inc} by calculating RMSE at each target pH. This comparison was used to evaluate the accuracy of standard SMP protocols and to quantify the extent to which machine-learning-based recommendations can reproduce or improve upon regional lime recommendation systems.

2.11 Reconstruction of predicted neutralization curves

Under deployment conditions, the trained model predicts pH gain as a function of soil descriptors and $CaCO_3$ application rate, but it does not directly return a complete neutralization curve. A curve reconstruction step was therefore introduced to recover the predicted soil-specific pH response across a continuous, agronomically relevant range of lime rates. For a given soil, the model was evaluated over a monotonically increasing vector of candidate $CaCO_3$ rates,

$$\mathbf{x} = \{\boldsymbol{x_1}, \boldsymbol{x_2}, \dots, \boldsymbol{x_N}\}, \qquad \boldsymbol{x_1} = \mathbf{0}, \quad \boldsymbol{x_{i+1}} > \boldsymbol{x_i},$$

yielding a corresponding sequence of predicted pH gains $\widehat{\boldsymbol{\Delta pH}}(\boldsymbol{x_i})$, for i =1,…, N. Predicted absolute pH values were then reconstructed as $\widehat{\boldsymbol{pH}}(\boldsymbol{x_i}) = \boldsymbol{pH_0} + \widehat{\boldsymbol{\Delta pH}}(\boldsymbol{x_i})$, where pH_0 is the initial soil pH. The resulting sequence constitutes an empirical predicted neutralization curve for the soil under consideration. To ensure that the reconstructed curve spanned the agronomically relevant domain, the upper limit of the $CaCO_3$ rate vector was determined from a predefined ceiling pH value $\boldsymbol{pH_{ceil}}$. Specifically, the smallest rate $\boldsymbol{x_{ceil}}$ such that (Eq. 13)

$$\boldsymbol{f(x) = \widehat{pH}(x) - pH_{ceil} \geq 0}. \quad (\mathbf{13})$$

was identified. Under the assumption that the predicted neutralization response is monotonic with increasing lime rate, this corresponds to a one-dimensional threshold-crossing problem. In practice, two complementary numerical strategies were evaluated: incremental threshold scanning and bracketed root finding. To prevent unrealistic extrapolation in cases where $\widehat{\boldsymbol{pH}}(\boldsymbol{x})$ did not reach $\boldsymbol{pH_{ceil}}$ within a plausible agronomic range, a maximum allowable rate $\boldsymbol{x_{max}}$was also imposed. The effective upper bound of the reconstructed rate domain was therefore defined as (Eq. 14)

$$\boldsymbol{x_{upper} = min(x_{ceil}, x_{max})}, \quad (\mathbf{14})$$

Once the interval $[\mathbf{0}, \boldsymbol{x_{upper}}]$ had been defined, the reconstructed curve was used to infer the lime rate required to reach any target pH such that $\boldsymbol{pH_{target} \leq pH_{ceil}}$. This inversion could be performed directly on the sampled response or after fitting a compact monotonic function, such as the Mitscherlich model, to stabilize the estimation. In this way, curve reconstruction and LR estimation were treated as two consecutive steps of the same inference framework: first recovering the predicted neutralization response, and then extracting the lime rate associated with any user-defined target pH.

3. Results

3.1. Comparative performance of chemical, spectral, and hybrid models for pointwise prediction of pH gain

All models evaluated in this study were able to predict soil pH gain (ΔpH) with good overall accuracy across the full set of soil × $CaCO_3$ rate combinations (Table 3). However, clear differences in predictive performance emerged across the types and levels of input information, allowing a consistent hierarchy to be established among model families. Overall, models based on detailed pedological characterization (DPC and DPC+) achieved the highest performance, followed closely by hybrid models combining chemical and spectral information. Models relying solely on routine chemical analyses (RC and RC+) also showed strong predictive ability, comparable to that of

mid-infrared spectral models (MIR). Among spectral approaches, MIR consistently outperformed visible–near-infrared (VisNIR) models, which showed lower predictive performance.

In contrast, minimal models, including the SMP-only model and the dual-pH model (pHwater–pHSMP), performed substantially worse than all other approaches (Table 3). It is important to note that the SMP and dual-pH models considered in this section were recalibrated on the present incubation dataset, and therefore do not correspond to the regional SMP-based recommendation tables currently used in Québec and Ontario. These operational recommendation systems are evaluated separately in a later section. A more detailed interpretation based on complementary performance criteria further clarifies this hierarchy. In terms of precision and as shown in Table 3, the best-performing models exhibited RMSE values of approximately 0.23–0.26 pH units, whereas VisNIR and minimal models showed higher errors, reaching approximately 0.31 and 0.35–0.39 pH units, respectively. Robustness, assessed by the coefficient of determination (R^2), followed the same pattern, with values exceeding 0.90 for the DPC, hybrid, RC, and MIR models, indicating a high level of predictive performance, while the VisNIR and minimal models remained below this threshold. Model exactitude, evaluated through regression slope and intercept (Fig. 4), showed that DPC, RC, and MIR models effectively captured the magnitude and structure of ΔpH variations, with slopes generally close to or above 0.90 and intercepts below 0.10.

In contrast, VisNIR models exhibited slightly lower slopes, indicating a reduced ability to reproduce the full amplitude of pH changes. Despite these differences, systematic bias remained low across all models, with mean prediction errors close to zero. The RPIQ metric further confirmed the relative predictive performance of the best models, with values exceeding 5 for DPC, RC, and MIR, compared with lower values for VisNIR and minimal models.

Table 3.
Predictive performance of all machine-learning models evaluated for pointwise prediction of soil pH gain under independent hold-out testing and 10-fold cross-validation.

Model	R^2_a	$RMSE_a$	$RPIQ_a$	$slope_a$	$intercept_a$	R^2_b	$RMSE_b$	$RPIQ_b$	$slope_b$	$intercept_b$
MIR	0.879	0.307	4.826	0.852	0.081	0.903	0.257	5.171	0.93	0.072
VisNIR	0.841	0.351	4.217	0.833	0.106	0.856	0.313	4.253	0.884	0.101
DPC+	0.898	0.274	5.268	0.898	0.086	0.921	0.232	5.74	0.916	0.081
DPC	0.896	0.277	5.213	0.896	0.088	0.921	0.239	5.558	0.914	0.087
RC+	0.882	0.303	4.883	0.865	0.098	0.902	0.259	5.143	0.9	0.096
RC	0.88	0.305	4.846	0.868	0.097	0.9	0.26	5.108	0.902	0.096

SMP	0.8	0.394	3.759	0.779	0.144	0.823	0.347	3.836	0.838	0.15
dual-pH(pH_{water}-pH_{SMP})	0.8	0.394	3.758	0.779	0.144	0.823	0.346	3.839	0.838	0.149
MIR-DPC+	0.908	0.262	5.524	0.893	0.068	0.918	0.232	5.633	0.935	0.063
MIR-DPC	0.896	0.284	5.218	0.871	0.074	0.921	0.231	5.75	0.933	0.065
MIR-RC+	0.893	0.288	5.145	0.859	0.082	0.914	0.242	5.504	0.931	0.072
MIR-RC	0.893	0.288	5.145	0.859	0.082	0.914	0.242	5.504	0.931	0.072
MIR-pH_{water}	0.887	0.296	4.999	0.86	0.085	0.91	0.247	5.381	0.936	0.064
VisNIR-DPC+	0.9	0.278	5.316	0.887	0.076	0.918	0.237	5.622	0.922	0.073
VisNIR-DPC	0.902	0.276	5.359	0.888	0.079	0.919	0.234	5.682	0.927	0.067
VisNIR-RC+	0.88	0.306	4.842	0.87	0.104	0.903	0.257	5.176	0.917	0.079
VisNIR-RC	0.887	0.296	5.003	0.878	0.099	0.903	0.257	5.176	0.916	0.081
VisNIR-pH_{water}	0.852	0.34	4.359	0.856	0.099	0.876	0.291	4.574	0.904	0.087
MIR-VisNIR	0.869	0.319	4.633	0.831	0.083	0.903	0.256	5.186	0.922	0.074
MIR-VisNIR-DPC+	0.891	0.291	5.085	0.882	0.06	0.916	0.24	5.549	0.931	0.064
MIR-VisNIR-DPC	0.901	0.277	5.34	0.872	0.074	0.914	0.242	5.505	0.927	0.07
MIR-VisNIR-RC+	0.88	0.305	4.857	0.841	0.078	0.903	0.257	5.172	0.925	0.072
MIR-VisNIR-RC	0.876	0.31	4.767	0.845	0.071	0.896	0.265	5.013	0.932	0.065
MIR-VisNIR-pH_{water}	0.876	0.31	4.767	0.845	0.071	0.896	0.265	5.013	0.932	0.065

a: denotes independent hold-out evaluation (20% of soils); **b** denotes 10-fold cross-validation across the full dataset. **R^2**: coefficient of determination; **RMSE**: root mean squared error; **RPIQ**: ratio of performance to interquartile distance; **slope** and **intercept**: parameters of the regression between observed and predicted ΔpH; **MIR:** mid-infrared spectroscopy**; VisNIR:** visible–near infrared spectroscopy**; DPC:** detailed pedological characterization**; RC:** routine chemistry**; SMP:** model using SMP buffer pH and $CaCO_3$ rate**; dual-pH:** model using both pH_{water} and pH_{SMP} together with $CaCO_3$ rate. + indicates inclusion of SMP buffer pH within the corresponding chemical feature set.

402

403 The regression diagnostics shown in Fig. 4 visually highlight these differences, with the DPC and MIR models
404 showing the closest alignment to the 1:1 line and the lowest dispersion across the full range of ΔpH values. RC
405 models exhibited a similar behavior, while VisNIR models showed greater scatter, particularly at higher pH gains.

406 Feature importance analysis provides insight into the underlying drivers of model performance. For spectral
407 models (Fig. 5), MIR-based predictions relied on information distributed across a wide spectral domain,
408 suggesting a comprehensive integration of soil properties related to acidity neutralization. In contrast, VisNIR
409 models depended on more localized spectral regions, which may explain their lower and less stable performance.
410 For chemical models (Fig. 6), the $CaCO_3$ application rate was consistently the dominant predictor, followed by key
411 soil properties such as initial pH, SOM, and CEC in DPC models, or Mehlich-3 extractable elements in RC models.
412 These results indicate that accurate prediction of ΔpH requires a coherent combination of descriptors that reflect

both soil buffering capacity and initial acidity. Minimal models, including the SMP-only and dual-pH models, performed significantly worse, with higher RMSE and lower R^2 values. Although these models capture some information about soil acidity, their limited number of predictors limits their ability to capture the complexity of soil neutralization processes.

Hybrid models combining chemical and spectral predictors generally improved predictive performance relative to single-domain models. In particular, combinations involving MIR and DPC (MIR–DPC and MIR–DPC+) achieved the highest overall performance. However, these gains were sometimes marginal compared with DPC alone, suggesting that spectral information may become partially redundant when detailed pedological descriptors are already available. Taken together, these results indicate that no single model provides a universally optimal solution. Rather, the different model families define a structured range of predictive options adapted to varying analytical contexts. DPC models offer the highest performance when detailed soil characterization is available, whereas RC models provide a robust and immediately transferable solution based on routine analyses. MIR models emerge as the most effective spectral alternative, combining strong predictive performance with high potential for rapid deployment. In contrast, VisNIR models and minimal approaches based on SMP or dual-pH measurements remain less performant but may still be relevant in contexts with limited analytical capacity.

3.2. Reconstruction of incubation-derived neutralization curves

The results presented in Section 3.1 showed that the different models accurately predicted pH gain (ΔpH) across the full set of soil × $CaCO_3$ rate combinations. However, the agronomic relevance of these models primarily lies in their ability to reconstruct, for a given soil, the complete neutralization response as a function of CaCO3 application. This step represents a higher level of integration, in which pointwise predictions are combined to recover full soil-specific neutralization curves.

The variability of these curves can be interpreted in light of the parameters of the Mitscherlich model fitted to the incubation data, summarized in Table 4. The parameters A and k describing the asymptotic pH gain and the rate of approach to this asymptote, respectively, exhibit substantial variability across soils. This dispersion reflects the heterogeneity of buffering behavior and neutralization dynamics within the dataset, and provides a useful framework for interpreting differences in reconstruction performance among models. The reconstructed profiles

shown in Fig. 7 can therefore be viewed as predictive approximations of these Mitscherlich-type responses, allowing a direct comparison between observed and reconstructed curve shapes. Within this framework, soil-specific predictors were held constant, and each model was used to predict ΔpH across the range of $CaCO_3$ application rates. This approach enabled the reconstruction of complete neutralization profiles for each soil, directly comparable to the observed incubation curves.

Table 4.
Descriptive statistics of Mitscherlich parameters (A and k) across the studied soils.

	A	**k**
mean	3.90	0.100
std	3.04	0.132
min	0.39	0.003
Q1	2.13	0.038
Q2	2.94	0.074
Q3	3.87	0.126
max	12.00	2.010
skewness	1.80	8.733
kurtosis	2.17	115.606

A: asymptotic maximum pH change (ΔpH) predicted by the Mitscherlich model. **k**: neutralization rate constant controlling the curvature of the ΔpH/$CaCO_3$ response. **mean**: arithmetic mean; **std**: standard deviation; **min**: minimum; **max**: maximum; **Q1**: first quartile (25th percentile); **Q2**: median (50th percentile); **Q3**: third quartile (75th percentile). **ΔpH**: change in soil pH relative to the initial soil pH before $CaCO_3$ addition.

Fig. 7 presents representative examples of reconstructed curves for the MIR, VisNIR, DPC, and RC models, corresponding to different levels of reconstruction error, namely the minimum, first quartile (Q1), median, third quartile (Q3), and maximum RMSE values. This representation provides a concise overview of model performance across the full dataset, without requiring inspection of individual curves. For low-error cases (minimum, Q1, and

median RMSE), all models exhibited excellent agreement with observed neutralization trajectories. Predicted curves closely followed the experimental responses across the full range of $CaCO_3$ rates, capturing both the initial rapid increase in pH and the progressive approach to a plateau. In these situations, differences among models were minimal, indicating that accurate pointwise predictions translate directly into reliable reconstruction of complete response curves. As reconstruction error increased (Q3), discrepancies between observed and predicted curves became more pronounced, particularly at higher $CaCO_3$ rates, where the progressive saturation of the response is more difficult to capture. Nevertheless, even under these conditions, the models generally preserved the overall shape of the curves, including the monotonic increase and the relative magnitude of ΔpH. The cases associated with the highest RMSE values highlight the most challenging soils in the dataset. In these extreme profiles, substantial deviations between observed and reconstructed curves were observed, both in the maximum ΔpH reached and in the rate of approach to the plateau. These situations are consistent with the strong variability observed in the Mitscherlich parameters, particularly the wide dispersion and skewness of k values reported in Table 4. Even under these conditions, chemical models (DPC and RC) showed greater reconstruction stability than purely spectral models, with lower maximum errors. In contrast, MIR, and especially VisNIR, exhibited greater variability in these extreme cases, suggesting increased sensitivity to atypical or highly nonlinear neutralization responses.

Overall, these results demonstrate that the quality of neutralization-curve reconstruction remains high for the majority of soils, with strong agreement between observed and predicted profiles. They confirm that the predictive performance at the pointwise ΔpH level is sufficient to recover complete soil-specific response functions reliably. This reconstruction capability constitutes a key step toward agronomic application, as it enables the estimation of a continuous relationship between soil pH and $CaCO_3$ application rate for each soil. It therefore provides a flexible basis for determining LRs across a range of target pH values, in contrast to traditional approaches that rely on fixed recommendation classes.

3.3. Inference-time reconstruction of predicted neutralization curves

The application of the models to a new soil differs fundamentally from the experimental incubation framework. In the dataset, each neutralization curve was observed at seven fixed $CaCO_3$ application rates. Under deployment conditions, however, these rates are not known a priori for a new soil, and the full neutralization curve must

494 therefore be reconstructed from model predictions over a dynamically defined range of $CaCO_3$ rates. As illustrated
495 in Fig. 8 and described in Section 2.11, this reconstruction is achieved by evaluating the model over a
496 monotonically increasing sequence of candidate $CaCO_3$ rates, thereby generating predicted pH gains across an
497 agronomically relevant range. The predicted ΔpH values are then converted into absolute pH values using the
498 initial soil pH (pH_0), obtained from routine soil analyses. This step enables the transition from pointwise
499 predictions of pH gain to a continuous pH/ $CaCO_3$ response curve that can be directly interpreted for agronomic
500 decision-making. The objective is therefore not to reproduce the original experimental rates, but to reconstruct,
501 for each new soil, a neutralization curve over a range of $CaCO_3$ rates that adequately spans agronomically relevant
502 target pH values and extends slightly beyond neutrality. As detailed in Section 2.11, the upper bound of this range
503 is defined using a ceiling-pH criterion so that the reconstructed curve covers the domain required for reliable LR
504 estimation while avoiding unrealistic extrapolation. In practice, the candidate rate domain was evaluated over a
505 discretized grid ($N=100$, $\Delta x=0.3$ t ha^{-1}), with the upper bound constrained to a maximum agronomically plausible
506 application rate of 50 t ha^{-1}. Under the assumption of a monotonic pH response with increasing $CaCO_3$ rate, the
507 threshold-crossing problem admits a unique solution, which was identified using either incremental threshold
508 scanning (ITS) or Brent's root-finding method.

509 Once the predicted curve has been reconstructed, the LR corresponding to any target pH can be derived by
510 inversion of the Mitscherlich relationship, following the framework presented in Section 2.4. In this sense, the
511 inference process can be viewed as a two-step procedure: first reconstructing the soil-specific neutralization
512 response over a relevant $CaCO_3$ rate range, and then extracting from this curve the $CaCO_3$ rate required to reach
513 a user-defined target pH. Within this context, the comparative evaluation of ITS and Brent's method was used to
514 quantify the computational efficiency of curve reconstruction under deployment conditions. This benchmarking
515 exercise reflects the time required for an end user to obtain, from a single soil sample, a complete reconstructed
516 neutralization curve together with the corresponding lime requirement prediction. Inference time varied
517 substantially depending on input dimensionality and inversion strategy. For spectral models using full-resolution
518 features, reconstruction required approximately 7.8 s per sample for VisNIR and 10.9 s for MIR using ITS, whereas
519 Brent's method required more than 100 s per sample in both cases. Application of the trimming and subsampling
520 protocol described in Section 2.5.1 reduced these times markedly, to approximately 1.2–1.6 s per sample with ITS

and 20–27 s per sample with Brent's method. In contrast, models based on chemical predictors required less than 0.1 s per sample with ITS and less than 3 s per sample with Brent's method. Across all configurations, ITS consistently outperformed Brent's method, with the largest advantage observed for high-dimensional spectral models.

Overall, these results demonstrate that inference-time reconstruction of predicted neutralization curves is not only feasible but also computationally efficient, particularly when using chemical predictors or preprocessed spectral inputs. Together with the workflow summarized in Fig. 8, they show that the proposed framework can be implemented in practice to generate soil-specific neutralization curves and derive lime requirements for flexible target pH values, thereby supporting a transition from discrete, table-based recommendations toward continuous, model-based decision systems.

3.4. Comparison of model-derived lime requirements with regional SMP-based recommendations

Fig. 9 compares the root mean squared errors (RMSEs) of LR estimates derived from the models developed in this study with those from the regional recommendation systems currently used in Québec and Ontario, across target pH values of 5.5, 6.0, 6.5, and 7.0. This comparison provides a direct assessment of the extent to which model-based reconstruction of neutralization curves can improve LR estimation relative to conventional table-based approaches. It is important to distinguish here between two categories of SMP-based approaches. On the one hand, the SMP and dual-pH models presented in this study correspond to minimal models recalibrated on the present incubation dataset. On the other hand, the values labeled Québec and Ontario in Fig. 9 correspond to regional tabular recommendations derived from previously established calibration tables or charts, which remain in operational use for estimating LRs at predefined target pH levels. The former therefore represent data-driven recalibration based on current observations, whereas the latter reflect legacy recommendation systems derived from earlier regional calibrations. Overall, LR estimates derived from models trained on incubation data consistently showed lower RMSE values than those from regional SMP-based recommendation tables across all target pH values. This trend indicates that approaches based on continuous reconstruction of neutralization curves provide a more accurate representation of soil behavior than fixed tabular systems. Among the evaluated models, those based on DPC exhibited the lowest errors throughout, with RMSE increasing from 0.86 t ha^{-1} at pH 5.5 to 2.98 t ha^{-1} at pH 7.0. RC models followed closely, with RMSE values increasing from 0.96 t ha^{-1} at pH 5.5 to 3.41 t ha^{-1} at pH 7.0. These results indicate that the most accurate LR estimates were obtained from models that

incorporated either detailed pedological information or routine chemistry, and that the performance advantage of these models was maintained even at the highest target pH values. The spectral models (MIR and VisNIR) showed a more contrasted pattern relative to RC. At lower target pH values (5.5 and 6.0), they remained competitive, with RMSE values generally below 1.5 t ha $^{-1}$. However, this ranking reversed at higher target pH values. At pH 6.5, spectral-model errors were slightly higher than those of RC, and at pH 7.0 they increased sharply to values above 4 t ha−1, compared with 3.41 t ha−1 for the RC model. This pattern suggests that spectral-only approaches remain effective for moderate LRs but become less reliable when prediction depends strongly on the upper, asymptotic portion of the neutralization curve. The recalibrated SMP and dual-pH models occupied an intermediate position. While they remained less accurate than models relying on richer chemical or spectral information, they still outperformed the regional tabular recommendations. Their errors also increased steeply with target pH, exceeding 5 t ha^{-1} at pH 7.0. This result shows that even minimal recalibration based on current incubation data can improve predictive accuracy relative to legacy regional systems, although it does not match the performance of the more informative model families. The regional SMP-based recommendation systems for Québec and Ontario had the highest overall RMSE values, particularly at higher target pH values. At pH 6.5, RMSE reached approximately 3.8 t ha^{-1} for the Québec table and 4.5 t ha^{-1} for the Ontario table. At pH 7.0, LR estimates were available only from the Ontario recommendation system, for which RMSE exceeded 7 t ha^{-1}. These values were substantially higher than those obtained with any of the best-performing model-based approaches. Taken together, these results show that the models developed in this study do not simply reproduce existing recommendation systems, but provide a measurable improvement in predictive accuracy while also allowing flexible estimation for any target pH. More broadly, they support a transition from discrete, table-based recommendation frameworks toward continuous, model-based decision systems grounded in soil-specific neutralization responses.

4. Discussion

4.1. Toward precision liming: reliability, deployability, and practical relevance of neutralization curve reconstruction

The results clearly demonstrate that the machine-learning framework developed in this study extends beyond point prediction and provides a robust basis for precision liming through soil-specific reconstruction of neutralization response curves. By formulating the response as pH gain (ΔpH) rather than absolute pH, the models

capture the intrinsic buffering behavior of soils while explicitly accounting for initial soil pH as an input variable. This formulation isolates the soil's neutralization dynamics and aligns with classical concepts of buffer capacity, defined as the change in pH per unit of base added rather than as an absolute pH value (Godsey et al., 2007; Sikora and Moore, 2008). Across all evaluated models, ΔpH was predicted with high accuracy over a wide range of soils and $CaCO_3$ application rates, with a clear hierarchy in model performance (Table 3). Models based on detailed pedological characterization (DPC) achieved the highest predictive performance, followed by routine chemistry (RC), MIR, and VisNIR, while recalibrated SMP and dual-pH models showed comparatively lower accuracy. This hierarchy reflects the progressive level of information contained in each feature set and confirms that soil buffering behavior can be reliably inferred from both chemical and spectral signatures. Importantly, this predictive accuracy translates into reliable functional reconstruction of neutralization curves, as illustrated in Fig. 7, where predicted profiles closely match observed incubation responses across soils. This result demonstrates that the models do not merely fit pointwise observations but successfully capture the underlying shape and asymptotic behavior of soil neutralization responses. Such capability is critical for practical applications, where the objective is not only to predict individual values but to describe the full response trajectory of a soil to liming. A key contribution of this work is the explicit resolution of the deployment challenge for new soils. In practice, a new soil is never associated with predefined $CaCO_3$ application rates, and the full response curve must be reconstructed from limited input data. The proposed framework addresses this limitation by generating predictions over a dynamically defined rate domain, converting ΔpH into absolute pH using measured pH_0, and reconstructing a continuous pH/CaCO3 response curve before inversion. The overall workflow, summarized in Fig. 8, demonstrates how soil descriptors are translated into a complete, soil-specific response function, enabling LR estimation for any target pH without requiring experimental dose-response data for the soil under consideration. From an operational perspective, the feasibility of this approach is supported by the observed inference times. Despite the need to evaluate models over multiple candidate rates, the combination of efficient numerical strategies and spectral dimensionality reduction ensures that curve reconstruction and LR estimation remain computationally tractable. In particular, models based on routine chemistry or preprocessed spectral data achieve inference times compatible with laboratory workflows and decision-support applications. This confirms that the proposed framework is not only theoretically sound but also practically deployable.

Beyond methodological considerations, the agronomic implications of this approach are substantial. Traditional recommendation systems, particularly those based on SMP buffer methods, provide a single lime dose associated with a limited set of predefined target pH values. In contrast, reconstructing continuous neutralization curves transforms the target pH into a flexible decision variable. This shift is central to precision liming, as it allows producers and advisors to select target pH values based on crop requirements, economic considerations, and risk management. For instance, in crops sensitive to excessive liming, such as potato, avoiding overcorrection of soil pH is critical to prevent diseases such as common scab. The ability to derive the LR for any chosen pH level provides a level of control not achievable with conventional tabular systems.

This transition from fixed-dose recommendations to continuous, soil-specific response functions is further supported by the comparison with regional SMP-based systems (Fig. 9). The lower prediction errors obtained with model-based approaches, combined with their flexibility, highlight the limitations of legacy tabular systems and reinforce the relevance of dynamic modeling frameworks for modern soil fertility management. Taken together, these results demonstrate that the proposed approach provides a complete and operational solution for new soils, integrating accurate ΔpH prediction, neutralization curve reconstruction, and flexible LR estimation. This combination of robustness, deployability, and agronomic relevance supports a shift in liming practices in North America, from rigid, table-based systems toward adaptive, model-based strategies grounded in soil-specific behavior. It establishes a strong foundation for the development of precision liming tools.

4.2. Mechanistic interpretation of chemical and spectral controls governing ΔpH reconstruction

The variable importance patterns observed in this study indicate that the reconstruction of ΔpH is governed by predictors that are fully consistent with the known mechanisms of soil acidity neutralization. Across all model families, $CaCO_3$ application rate emerged as the dominant predictor, reflecting the inherently dose-dependent nature of liming. However, predictive performance was not driven solely by lime rate. The models' ability to accurately reconstruct neutralization curves depended critically on their capacity to capture the soil's initial chemical state, its buffering capacity, and the structure of its acidity pools. As shown in Figs. 5 and 6, the most performant models rely on combinations of variables that collectively describe these complementary dimensions.

In models based on detailed pedological characterization (DPC), the most influential predictors included CEC, initial soil pH, SOM content, texture, exchangeable acidity, and selected exchangeable cations. This set of variables captures multiple components of soil buffering systems. Among them, CEC plays a central role, as it integrates the density of exchange sites associated with clay minerals and SOM, thereby representing a fundamental determinant of resistance to pH changes (Sumner and Miller, 1996; Sparks, 2003). This interpretation is consistent with classical approaches to liming, in which buffering capacity has long been related to the size and composition of the exchange complex. Although such pedological characterization has sometimes been underutilized in routine recommendations due to higher analytical costs, it remains grounded in robust physicochemical principles. In this context, it is particularly noteworthy that the COMIFER (2009) framework reintroduced CEC and base saturation as central variables for lime recommendation in France, following observations that several acidity indicators exhibited significant variability depending on the timing of soil sampling. This shift toward more stable pedological descriptors underscores the need to rely on integrative variables that reflect soil structure rather than transient chemical states. The strong importance of CEC observed in the present study aligns with this perspective. It confirms that it remains one of the most effective descriptors of soil buffering behavior and neutralization dynamics. The importance of initial soil pH further reflects its role as a proxy for the chemical state of the system, controlling processes such as aluminum hydrolysis and the neutralization of variable-charge sites (Thomas and Hargrove, 1984; Curtin and Trolove, 2013). SOM also plays a major role, both through its functional groups, which carry pH-dependent charges, and through its interactions with aluminum, which strongly influence buffering behavior in acidic soils (Haynes and Naidu, 1998; Bloom et al., 1979). The simultaneous selection of clay content, exchangeable acidity, and ammonium acetate–extractable aluminum further confirms that DPC models capture multiple complementary components of the soil buffering system, rather than relying on a single proxy variable.

Models based on routine chemistry (RC) relied on a more parsimonious yet highly informative set of predictors, including initial pH, SOM, and Mehlich-3-extractable elements such as calcium and aluminum. The recurrence of these variables across model types is particularly significant, as they correspond to measurements widely available in routine soil testing laboratories. Their importance suggests that standard analytical datasets already contain a substantial portion of the information required to predict liming response. This observation is

consistent with our previous work on titration curves (Jouichat and Khiari, 2026), where similar variables were sufficient to reconstruct ΔpH. The fact that they re-emerge here under incubation conditions further supports their robustness as descriptors of soil neutralization behavior.

Spectral models capture these same controls more indirectly through signatures of mineralogy, organic matter, and physicochemical soil properties. The superior performance of MIR relative to VisNIR is consistent with the fact that the mid-infrared region is dominated by fundamental molecular vibrations, which are generally more chemically specific than the overtone and combination bands that characterize the VisNIR domain (Viscarra Rossel et al., 2006; Viscarra Rossel and Behrens, 2010; Ng et al., 2019, 2022). This difference is well established in soil spectroscopy and explains why MIR typically outperforms VisNIR for predicting chemically controlled soil properties. In the present study, the most informative MIR regions were consistent with absorptions associated with O–H functional groups in minerals and structural water, organic matter, and calcium- or carbonate-related environments, all of which are plausibly linked to soil buffering capacity and acid neutralization processes (Viscarra Rossel et al., 2006; Ng et al., 2022; Hume et al., 2022). Without over-interpreting individual bands, the overall pattern suggests that MIR captures an integrated signature of the mineral–organic system and its interaction with calcium, which explains its strong predictive performance. By contrast, the VisNIR domain appears to rely on broader and less chemically specific spectral features, particularly in the visible range, where soil color, iron oxides, and general pedogenic context dominate (Viscarra Rossel and Behrens, 2010; Viscarra Rossel et al., 2022). While these properties remain indirectly related to mineralogy and soil composition, their lower chemical specificity likely explains why VisNIR models reproduce neutralization responses less accurately, especially in the upper, asymptotic portion of the response curves, where precise characterization of buffering processes becomes critical.

Taken together, these results demonstrate that the most accurate models are not based on arbitrary predictors, but on variables that directly or indirectly represent the key components of soil buffering systems: initial acidity status, exchange site density, organic matter contribution, mineral surfaces, and exchangeable acidity pools. This mechanistic consistency reinforces the credibility of the proposed modeling framework. It explains the observed hierarchy of model performance, in which DPC, RC, and MIR models outperform VisNIR and minimal SMP-based approaches.

4.3. Implications for lime recommendation: moving beyond SMP-based tabular systems toward dynamic response models

The results of this study highlight fundamental limitations of lime recommendation systems based on tabular approaches, particularly those derived from SMP buffer pH. While these systems have historically provided simple, operational guidelines, they rely on discrete empirical relationships established for a limited number of target pH values and fail to capture the continuous variability in soil responses to liming. Direct comparison with current regional recommendation systems used in Québec and Ontario (Fig. 9) clearly shows that these approaches yield larger prediction errors than the models developed in this study, especially at higher target pH values, where LR estimation depends strongly on the response's curvature and asymptotic behavior. These limitations are not only methodological but also conceptual. Tabular systems reduce soil response to a static relationship between a single acidity indicator and a single lime rate. In contrast, the present results demonstrate substantial variability in soil-specific neutralization trajectories. The dispersion of Mitscherlich parameters (Table 4), particularly the asymptote A and curvature parameter k, confirms that soils differ not only in their maximum achievable pH correction but also in the rate at which this correction occurs. Such variability cannot be adequately represented by a single lookup table linking an acidity indicator to a recommended lime rate. The fragility of single-indicator systems is further reinforced by the variability and uncertainty inherent in acidity measurements. In a comprehensive study of the temporal variability of soil fertility indicators in Québec, Chelabi et al. (2021) showed that soil pH measured in water (pH_{water}) can exhibit clear seasonal patterns, depending on soil type and sampling period, potentially leading to inconsistent diagnostic interpretations. Although pH_{SMP} did not show a significant seasonal signal under the CEAEQ reproducibility criteria (CEAEQ, 2015), the authors emphasized that the accepted analytical tolerance for pH_{SMP} in Québec (±0.2 units) may translate into LR errors of approximately ±2.5 t ha^{-1}, which are difficult to account for in practical recommendations. They further highlighted that both pH_{water} and pH_{SMP}, despite their widespread use, remain incomplete indicators when used alone, and it is recommended to integrate additional soil properties, such as texture, SOM, exchangeable aluminum, and CEC, to improve acidity diagnosis and LR estimation. These observations are consistent with the findings of the present study, where the most accurate models are those that move beyond single-indicator approaches and instead reconstruct a full soil response based on a broader set of descriptors. The proposed framework explicitly addresses this limitation by reintroducing the soil-specific neutralization curve as the

central element of lime recommendation. By combining predicted ΔpH responses (Table 3), reconstructed response profiles (Fig. 7), and an operational inference pipeline (Fig. 8), it is possible to derive LRs for any target pH without relying on predefined classes or tabular thresholds. This transition from a discrete to a continuous framework represents a major advancement. A fixed recommendation system no longer determines the target pH but becomes a flexible decision variable that can be adjusted to meet agronomic, economic, or environmental objectives. From a practical perspective, this shift has important implications for lime management systems in North America. Rather than prescribing a single rate derived from a static reference, the proposed approach provides a soil-specific response function, allowing users to explore multiple liming scenarios and select an appropriate target pH based on their specific constraints. This aligns closely with the principles of precision agriculture, where management decisions are increasingly tailored to site-specific conditions and production goals. Importantly, this transition does not rely on a single analytical pathway. The strength of the proposed framework lies in its flexibility, which allows different sources of soil information to be used within the same conceptual framework of curve-based recommendations. The key shift is therefore not from one analytical method to another, but from a static, indicator-based system to a dynamic, response-based paradigm that explicitly represents soil behavior under liming. The performance comparison of LR predictions (Fig. 9) further demonstrates that this approach not only provides conceptual improvements but also delivers measurable gains in predictive accuracy. In this context, dynamic models offer a robust alternative to conventional SMP-based systems, reducing reliance on buffer pH measurements while maintaining or improving recommendation precision.

Overall, this study demonstrates that moving from tabular lime recommendations toward continuous, soil-specific response functions is both feasible and desirable. By explicitly accounting for soil variability, reducing dependence on single acidity indicators, and enabling flexible target pH selection, this approach lays the foundation for a new generation of lime recommendation systems better aligned with the requirements of precision agriculture and sustainable soil management.

5. Conclusion

This study demonstrates that LR can be determined from a fundamentally different perspective: not as a function of a single acidity indicator, but as the outcome of a soil-specific neutralization response reconstructed across amendment rates. By combining machine learning with Mitscherlich-type modeling, we show that soil acidity correction can be expressed as a continuous response function that captures both the magnitude and dynamics of pH change. The key contribution is not merely improved predictive performance over conventional SMP-based systems, but a redefinition of the recommendation framework itself. Liming is no longer treated as a fixed mapping between an indicator and a single rate, but as a dose–response relationship that allows flexible selection of target pH values and adaptation to agronomic, economic, and environmental constraints. This shift places soil behavior, rather than empirical tables, at the center of decision-making. A critical outcome of this work is the demonstration that such an approach is operationally deployable. Neutralization curves can be reconstructed for new soils using readily available chemical or spectral descriptors, without requiring experimental dose-response measurements. This enables direct estimation of LR for any desired target pH, making the framework compatible with real-world laboratory and advisory contexts.

Taken together, these results establish a transition from static, table-based recommendations toward dynamic, data-driven liming strategies. By explicitly accounting for soil variability and enabling flexible decision-making, this approach provides a foundation for next-generation soil acidity management systems aligned with the principles of precision agriculture.

Declaration of competing interest

The authors declare that they have no known competing financial interests or personal relationships that could have appeared to influence the work reported in this paper.

Acknowledgments

This work is a key component of the DAQARA project, generously supported by NSERCC and four industrial partners: Rio Tinto, Graymont, Omya, and OCP-Africa.

References

Adams, F. (Ed.), 1984. Soil Acidity and Liming, second ed. Agronomy Monograph 12. ASA, CSSA, and SSSA, Madison, WI. https://doi.org/10.2134/agronmonogr12.2ed

763 Akiba, T., Sano, S., Yanase, T., Ohta, T., Koyama, M., 2019. Optuna: A next-generation hyperparameter optimization
764 framework, in: Proceedings of the 25th ACM SIGKDD International Conference on Knowledge Discovery & Data
765 Mining. ACM, New York, NY, pp. 2623–2631. https://doi.org/10.1145/3292500.3330701
766 Alley, M.M., Zelazny, L.W., 1987. Soil acidity: Soil pH and lime needs, in: Brown, J.R. (Ed.), Soil Testing: Sampling,
767 Correlation, Calibration, and Interpretation. SSSA Special Publication 21. SSSA, Madison, WI, pp. 65–72.
768 https://doi.org/10.2136/sssaspecpub21.c7
769 Altmann, A., Toloşi, L., Sander, O., Lengauer, T., 2010. Permutation importance: A corrected feature importance
770 measure. Bioinformatics 26, 1340–1347. https://doi.org/10.1093/bioinformatics/btq134
771 Barnes, R.J., Dhanoa, M.S., Lister, S.J., 1989. Standard normal variate transformation and de-trending of near-
772 infrared diffuse reflectance spectra. Appl. Spectrosc. 43, 772–777. https://doi.org/10.1366/0003702894202201
773 Bloom, P.R., McBride, M.B., Weaver, R.M., 1979. Aluminum organic matter in acid soils: buffering and solution
774 aluminum activity. Soil Sci. Soc. Am. J. 43, 488–493.
775 https://doi.org/10.2136/sssaj1979.03615995004300030012x
776 Breiman, L., 2001. Random forests. Mach. Learn. 45, 5–32. https://doi.org/10.1023/A:1010933404324
777 Brent, R.P., 1971. An algorithm with guaranteed convergence for finding a zero of a function. Comput. J. 14, 422–
778 425. https://doi.org/10.1093/comjnl/14.4.422
779 Centre d'expertise en analyse environnementale du Québec (CEAEQ), 2014. Détermination du pH : méthode
780 électrométrique (MA. 100 – pH 1.1), éd. rév. Ministère du Développement durable, de l'Environnement et de la
781 Lutte contre les changements climatiques du Québec, Québec, QC.
782 Centre d'expertise en analyse environnementale du Québec (CEAEQ), 2015. Critères de variation relatifs, DR-12-
783 CVR. Ministère du Développement durable, de l'Environnement et de la Lutte contre les changements climatiques,
784 Québec, QC.
785 Chelabi, H., Khiari, L., Gallichand, J., 2021. Temporal variability of soil fertility indicators and sampling periods in
786 Québec. Can. J. Soil Sci. 102, 549–559. https://doi.org/10.1139/cjss-2021-0079
787 COMIFER (Groupe Chaulage), 2009. Le chaulage : des bases pour le raisonner. ARVALIS-Institut du végétal, Paris,
788 France.
789 Centre de référence en agriculture et agroalimentaire du Québec (CRAAQ), 2010. Guide de référence en
790 fertilisation, 2nd ed. CRAAQ, Québec, QC.

Conseil des productions végétales du Québec (CPVQ), 1997. Méthodes d'analyse des sols, des fumiers et des tissus végétaux. CPVQ, Québec, QC.

Curtin, D., Trolove, S., 2013. Predicting pH buffering capacity of New Zealand soils from organic matter content and mineral characteristics. Soil Res. 51, 494–502. https://doi.org/10.1071/SR13137

Day, P.R., 1965. Particle fractionation and particle-size analysis, in: Black, C.A. (Ed.), Methods of Soil Analysis: Part 1 Physical and Mineralogical Properties. American Society of Agronomy, Madison, WI, pp. 545–567.

Fageria, N.K., Baligar, V.C., 2008. Ameliorating soil acidity of tropical Oxisols by liming for sustainable crop production. Adv. Agron. 99, 345–399. https://doi.org/10.1016/S0065-2113(08)00407-0

Follett, R.H., Follett, R.F., 1983. Soil and lime requirement tests for the 50 states and Puerto Rico. J. Agron. Educ. 12, 9–17. https://doi.org/10.2134/jae.1983.0009

Godsey, C.B., Pierzynski, G.M., Mengel, D.B., Lamond, R.E., 2007. Evaluation of common lime requirement methods. Soil Sci. Soc. Am. J. 71, 843–850. https://doi.org/10.2136/sssaj2006.0121

Goulding, K.W.T., 2016. Soil acidification and the importance of liming agricultural soils with particular reference to the United Kingdom. Soil Use Manag. 32, 390–399. https://doi.org/10.1111/sum.12270

Guyon, I., Weston, J., Barnhill, S., Vapnik, V., 2002. Gene selection for cancer classification using support vector machines. Mach. Learn. 46, 389–422. https://doi.org/10.1023/A:1012487302797

Haynes, R.J., Naidu, R., 1998. Influence of lime, fertilizer and manure applications on soil organic matter content and soil physical conditions: a review. Nutr. Cycl. Agroecosyst. 51, 123–137. https://doi.org/10.1023/A:1009738307837

Hume, R., Marschner, P., Schilling, R.K., Mason, S., Mosley, L.M., 2022. Detection of agriculturally relevant lime concentrations in soil using mid-infrared spectroscopy. Geoderma 409, 115639. https://doi.org/10.1016/j.geoderma.2021.115639

International Agency for Research on Cancer (IARC), 2012. A Review of Human Carcinogens: Arsenic, Metals, Fibres, and Dusts. IARC Monographs on the Evaluation of Carcinogenic Risks to Humans, Vol 100C. IARC, Lyon, France.

Jouichat, H., Khiari, L., 2026. Reconstructing soil acidity neutralization curves using Machine learning and chemical or spectral soil signatures. Geoderma 465, 117645. https://doi.org/10.1016/j.geoderma.2026.117645

Kissel, D.E., West, L.T., Adkins, W., Cabrera, M., 2007. Soil pH and lime requirement, in: Kansas State University (Ed.), Soil Testing and Plant Analysis. Manhattan, KS.

Lavkulich, L.M., 1981. Methods Manual, Pedology Laboratory. Department of Soil Science, University of British Columbia, Vancouver, BC.

Lemire, E., Taillon, K.M., Hendershot, W.H., 2006. Using pH-dependent CEC to determine lime requirement. Can. J. Soil Sci. 86, 133–139. https://doi.org/10.4141/S05-002

Levenberg, K., 1944. A method for the solution of certain nonlinear problems in least squares. Q. Appl. Math. 2, 164–168. https://doi.org/10.1090/qam/10666

Liu, M., Kissel, D.E., Vendrell, P.F., Cabrera, M.L., 2004. Soil lime requirement by direct titration with calcium hydroxide. Soil Sci. Soc. Am. J. 68, 1228–1233. https://doi.org/10.2136/sssaj2004.1228

Marquardt, D.W., 1963. An algorithm for least-squares estimation of nonlinear parameters. J. Soc. Ind. Appl. Math. 11, 431–441. https://doi.org/10.1137/0111030

McLean, E.O., Eckert, D.J., Reddy, G.Y., Trierweiler, J.F., 1978. An improved SMP soil lime requirement method incorporating double-buffer and quick-test features. Soil Sci. Soc. Am. J. 42, 311–316. https://doi.org/10.2136/sssaj1978.03615995004200020022x

Mehlich, A., 1984. Mehlich 3 soil test extractant: A modification of Mehlich 2 extractant. Commun. Soil Sci. Plant Anal. 15, 1409–1416. https://doi.org/10.1080/00103628409367568

Mitscherlich, E.A., 1909. Das Gesetz des Minimums und das Gesetz des abnehmenden Bodenertrages. Landwirtsch. Jahrb. 38, 537–552.

Munroe, J. (Ed.), 2018. Soil Fertility Handbook (Publication 611). Ontario Ministry of Agriculture, Food and Rural Affairs (OMAFRA), Toronto, ON.

National Institute for Occupational Safety and Health (NIOSH), 2013. Criteria for a Recommended Standard: Occupational Exposure to Hexavalent Chromium. DHHS (NIOSH) Publication No. 2013-112.

Nelson, D.W., Sommers, L.E., 1982. Total carbon, organic carbon, and organic matter, in: Page, A.L. (Ed.), Methods of Soil Analysis: Part 2 Chemical and Microbiological Properties. Agronomy Monograph 9. ASA and SSSA, Madison, WI, pp. 539–579. https://doi.org/10.2134/agronmonogr9.2.2ed.c29

Ng, W., Minasny, B., Jeon, S.H., McBratney, A., 2022. Mid-infrared spectroscopy for accurate measurement of an extensive set of soil properties for assessing soil functions. Soil Secur. 6, 100043. https://doi.org/10.1016/j.soisec.2022.100043

Ng, W., Minasny, B., Montazerolghaem, M., Padarian, J., Ferguson, R., Bailey, S., McBratney, A.B., 2019. Convolutional neural network for simultaneous prediction of several soil properties using visible/near-infrared, mid-infrared, and their combined spectra. Geoderma 352, 251–267. https://doi.org/10.1016/j.geoderma.2019.06.016

Pedregosa, F., Varoquaux, G., Gramfort, A., Michel, V., Thirion, B., Grisel, O., Blondel, M., Prettenhofer, P., Weiss, R., Dubourg, V., Vanderplas, J., Passos, A., Cournapeau, D., Brucher, M., Perrot, M., Duchesnay, É., 2011. Scikit-learn: Machine learning in Python. J. Mach. Learn. Res. 12, 2825–2830.

Quinlan, J.R., 1992. Learning with continuous classes, in: Proceedings of the 5th Australian Joint Conference on Artificial Intelligence. World Scientific, Singapore, pp. 343–348.

Rinnan, Å., van den Berg, F., Engelsen, S.B., 2009. Review of the most common pre-processing techniques for near-infrared spectra. TrAC Trends Anal. Chem. 28, 1201–1222. https://doi.org/10.1016/j.trac.2009.07.007

Savitzky, A., Golay, M.J., 1964. Smoothing and differentiation of data by simplified least squares procedures. Anal. Chem. 36, 1627–1639. https://doi.org/10.1021/ac60214a047

Shoemaker, H.E., McLean, E.O., Pratt, P.F., 1961. Buffer methods for determining lime requirement of soils with appreciable amounts of extractable aluminum. Soil Sci. Soc. Am. J. 25, 274–277. https://doi.org/10.2136/sssaj1961.03615995002500040014x

Sikora, F.J., 2006. A buffer that mimics the SMP buffer for determining lime requirement of soil. Soil Sci. Soc. Am. J. 70, 474–486. https://doi.org/10.2136/sssaj2005.0164

Sikora, F.J., Moore, K.P., 2008. The Moore–Sikora buffer for lime requirement determinations. Soil Sci. Soc. Am. J. 72, 1163–1173. https://doi.org/10.2136/sssaj2007.0268

Sparks, D.L., 2003. Environmental Soil Chemistry, second ed. Academic Press, San Diego, CA.

Sumner, M.E., Miller, W.P., 1996. Cation exchange capacity and exchange coefficients, in: Sparks, D.L. (Ed.), Methods of Soil Analysis: Part 3 Chemical Methods. SSSA Book Series 5. SSSA and ASA, Madison, WI, pp. 1201–1229.

871 Sumner, M.E., Noble, A.D., 2003. Soil acidification: the world story, in: Rengel, Z. (Ed.), Handbook of Soil Acidity.
872 Marcel Dekker, New York, NY, pp. 15–42.
873 Thomas, G.W., 1982. Exchangeable cations, in: Page, A.L. (Ed.), Methods of Soil Analysis: Part 2 Chemical and
874 Microbiological Properties. Agronomy Monograph 9. ASA and SSSA, Madison, WI, pp. 159–165.
875 Thomas, G.W., Hargrove, W.L., 1984. The chemistry of soil acidity, in: Adams, F. (Ed.), Soil Acidity and Liming,
876 second ed. Agronomy Monograph 12. ASA, CSSA, and SSSA, Madison, WI, pp. 3–56.
877 Tran, T.S., Van Lierop, W., 1982. Lime requirement determination for attaining pH 5.5 and 6.0 of coarse-textured
878 soils using buffer-pH methods. Soil Sci. Soc. Am. J. 46, 1008–1014.
879 https://doi.org/10.2136/sssaj1982.03615995004600050024x
880 Van Lierop, W., 1990. Soil pH and lime requirement determination, in: Westerman, R.L. (Ed.), Soil Testing and
881 Plant Analysis, third ed. SSSA Book Series 3. SSSA, Madison, WI, pp. 73–126.
882 Van Lierop, W., Tran, T.S., 1983. Détermination du besoin en chaux des sols minéraux et organiques par la
883 méthode SMP. Science et technique AGDEX 534. Ministère de l'Agriculture, des Pêcheries et de l'Alimentation du
884 Québec, Québec, QC.
885 Van Rossum, G., Drake, F.L., 2009. Python 3 Reference Manual. CreateSpace, Scotts Valley, CA.
886 Viscarra Rossel, R.A., Behrens, T., 2010. Using data mining to model and interpret soil diffuse reflectance spectra.
887 Geoderma 158, 46–54. https://doi.org/10.1016/j.geoderma.2009.12.025
888 Viscarra Rossel, R.A., Behrens, T., Ben-Dor, E., Chabrillat, S., Demattê, J.A.M., Ge, Y., Shen, Z., 2022. Diffuse
889 reflectance spectroscopy for estimating soil properties: A technology for the 21st century. Eur. J. Soil Sci. 73,
890 e13271. https://doi.org/10.1111/ejss.13271
891 Viscarra Rossel, R.A., Walvoort, D.J.J., McBratney, A.B., Janik, L.J., Skjemstad, J.O., 2006. Visible, near infrared, mid
892 infrared or combined diffuse reflectance spectroscopy for simultaneous assessment of various soil properties.
893 Geoderma 131, 59–75. https://doi.org/10.1016/j.geoderma.2005.03.007
894 von Uexküll, H.R., Mutert, E., 1995. Global extent, development and economic impact of acid soils. Plant Soil 171,
895 1–15. https://doi.org/10.1007/BF00009558
896 Walkley, A., Black, I.A., 1934. An examination of the Degtjareff method for determining soil organic matter, and a
897 proposed modification of the chromic acid titration method. Soil Sci. 37, 29–38.

898 Wolf, A.M., Watson, M.E., Wolf, N.A., 2008. Digestion and dissolution methods for P, K, Ca, Mg and trace elements,
899 in: Carter, M.R., Gregorich, E.G. (Eds.), Soil Sampling and Methods of Analysis, second ed. CRC Press, Boca Raton,
900 FL, pp. 605–616.
901 Woodruff, C.M., 1948. Testing soils for lime requirement by means of a buffered solution and the glass electrode.
902 Soil Sci. 66, 53–64.

Figure 1.pdf

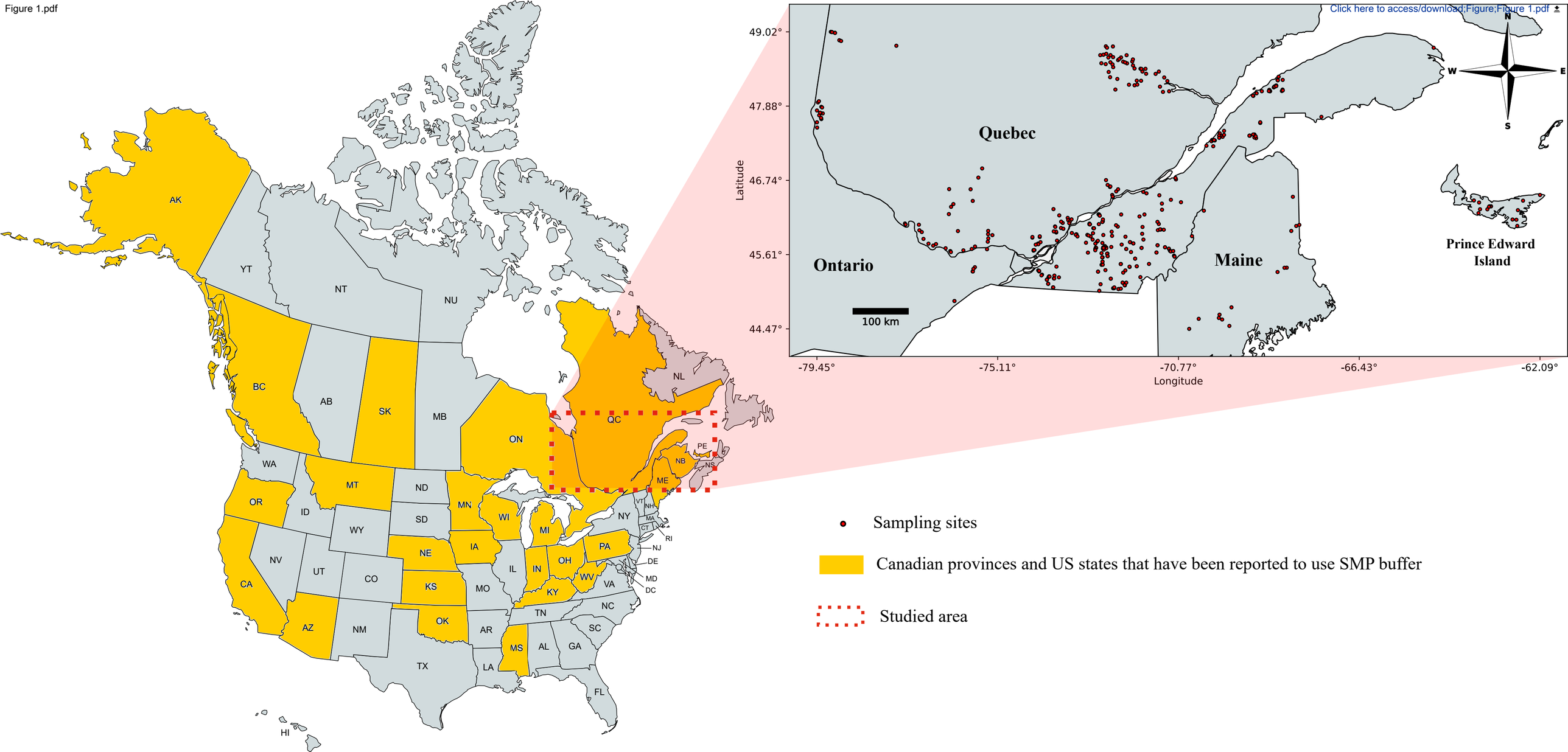

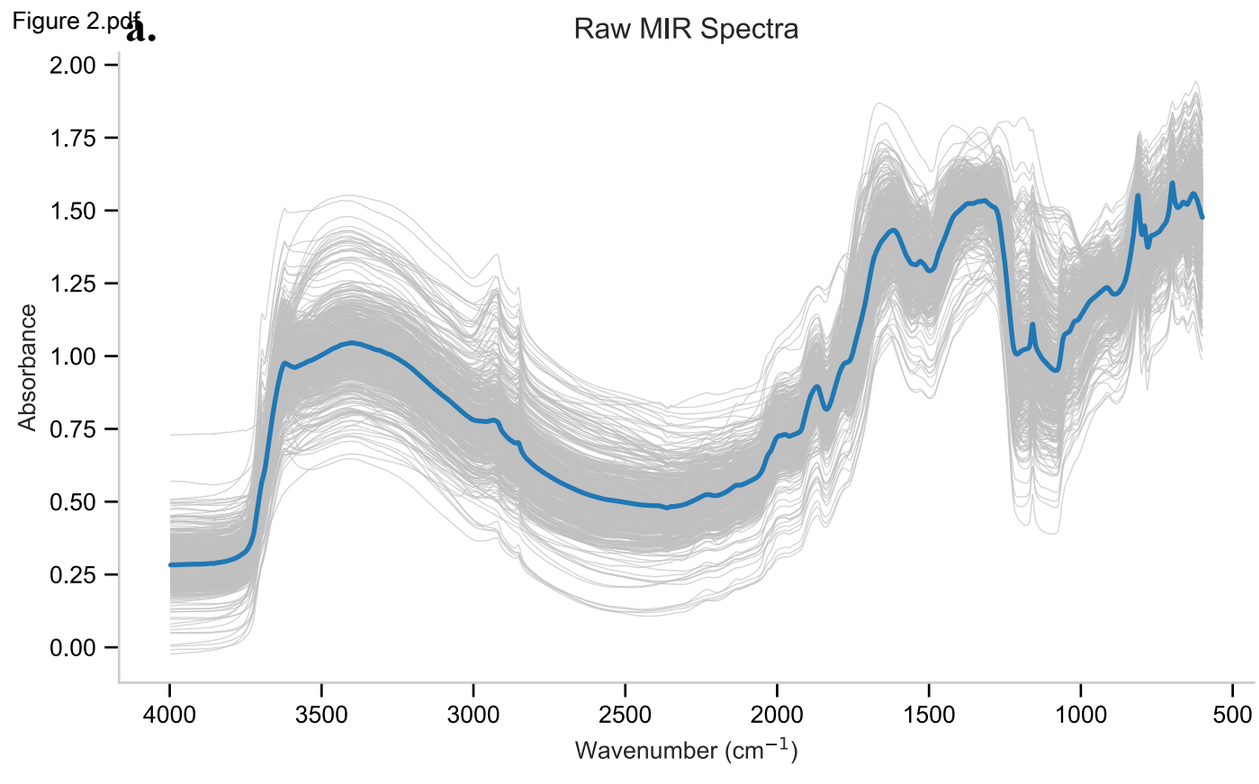

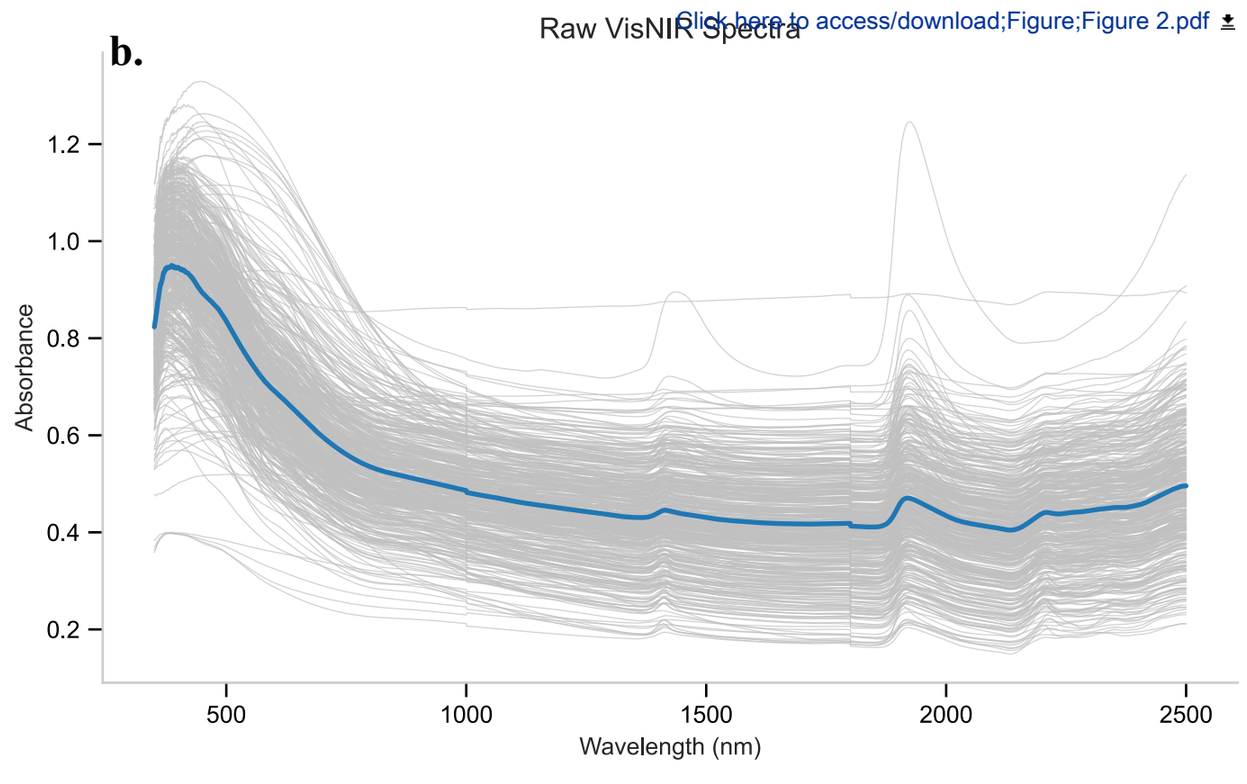

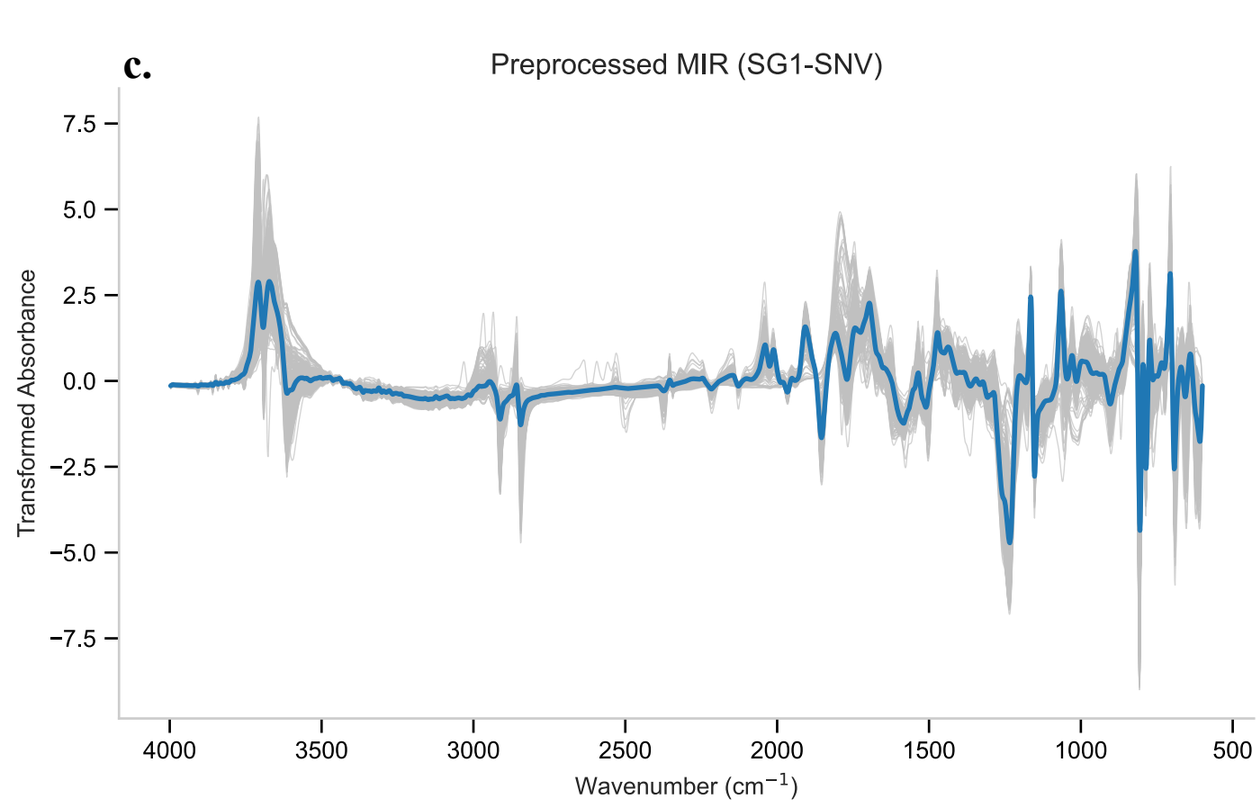

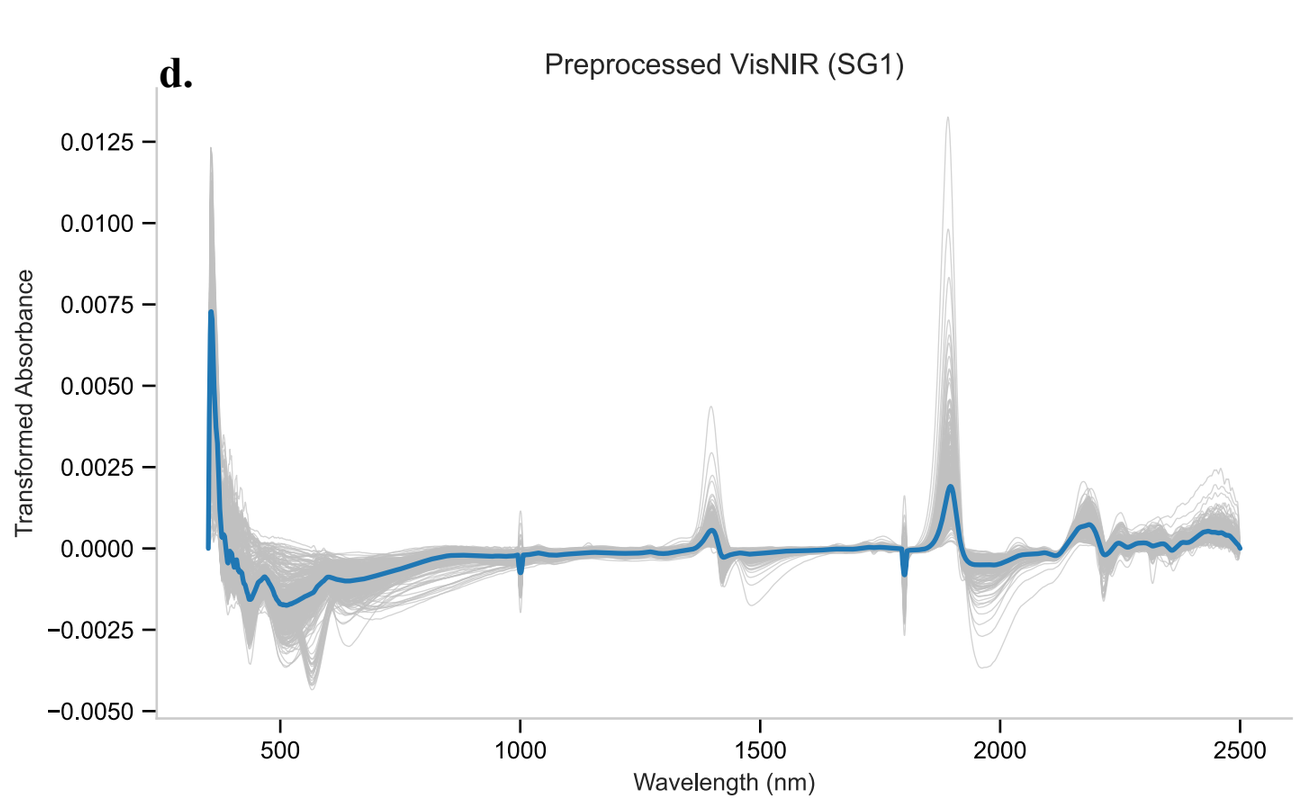

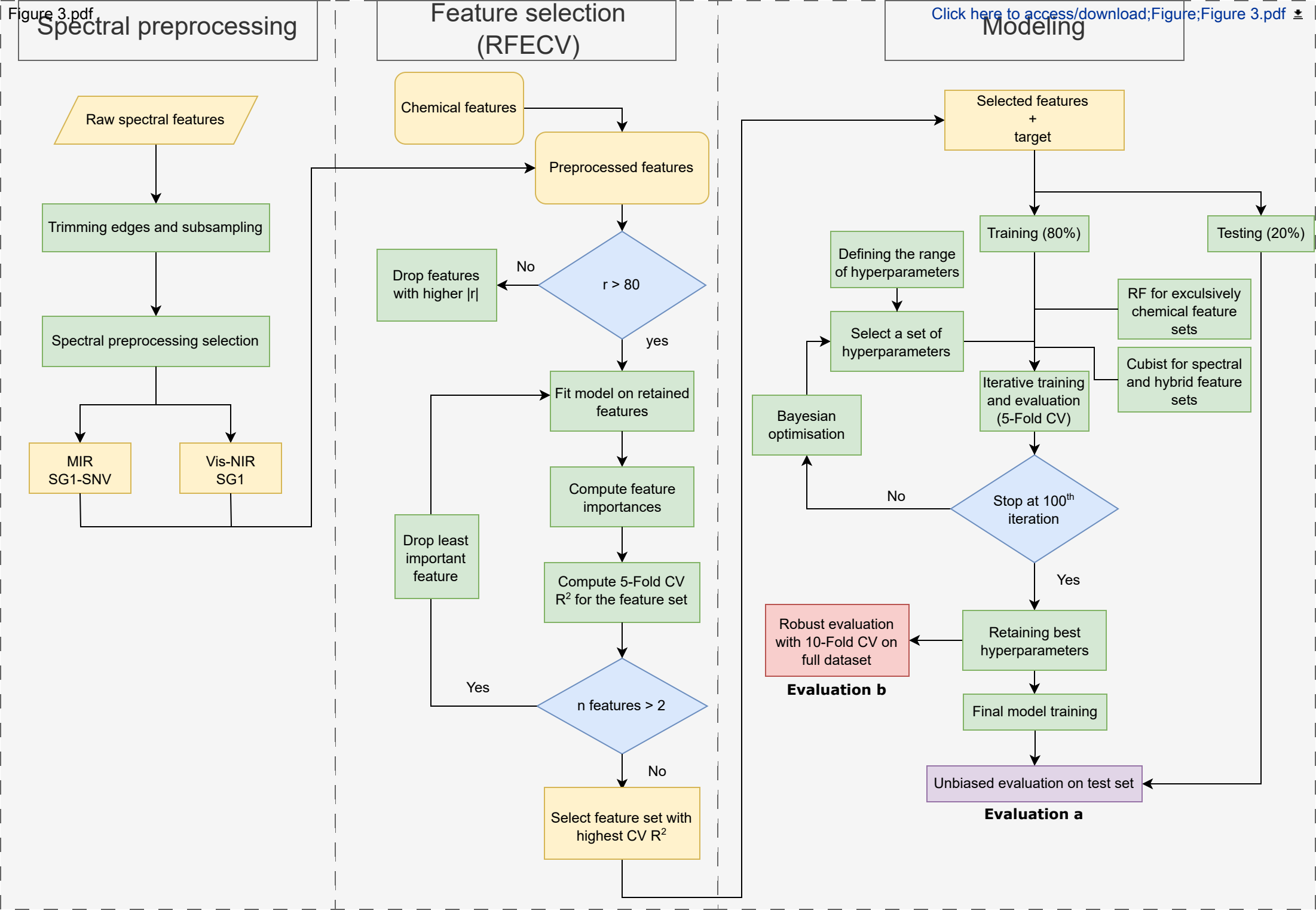

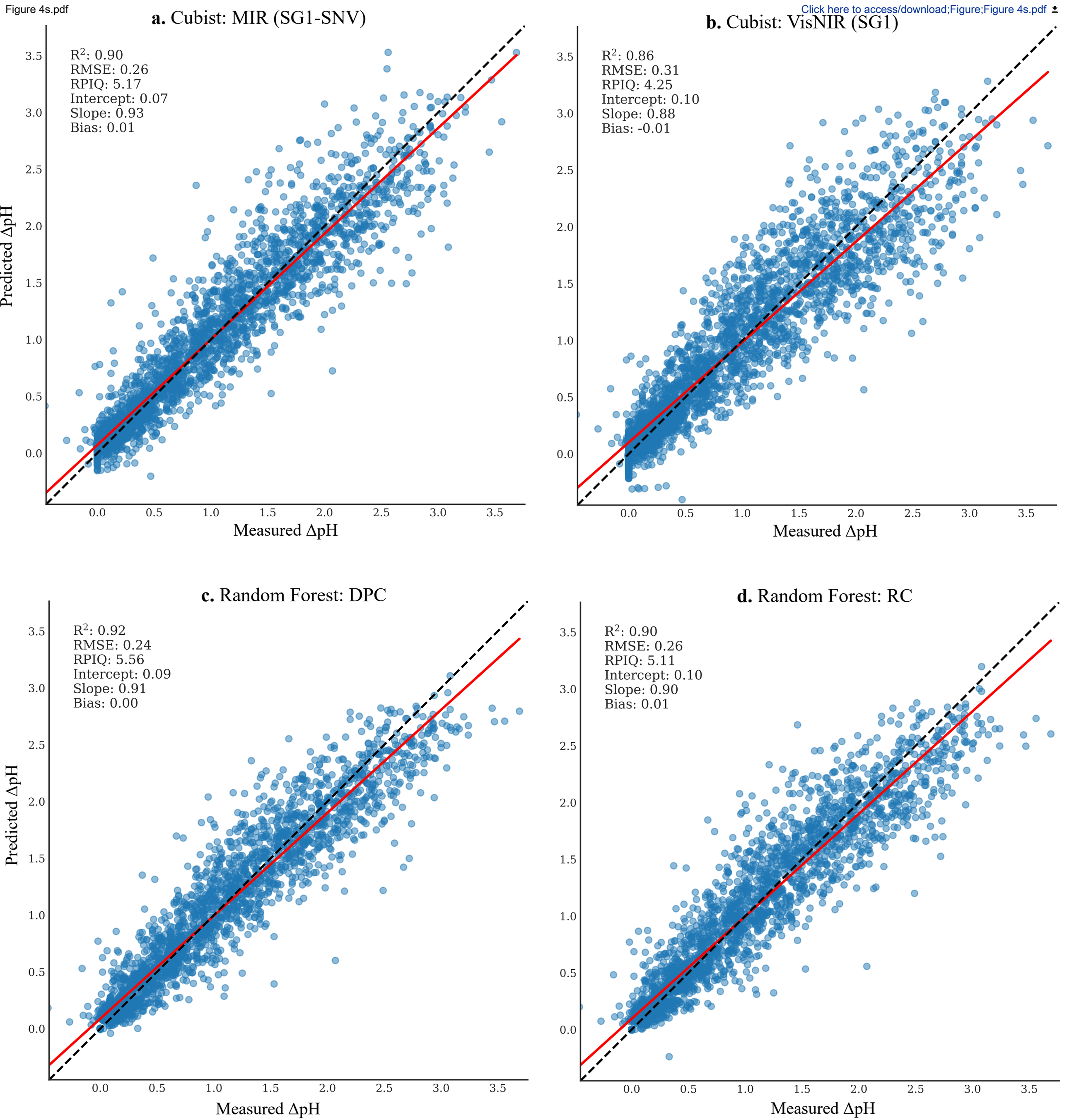

a. Importance of spectral features (MIR model)

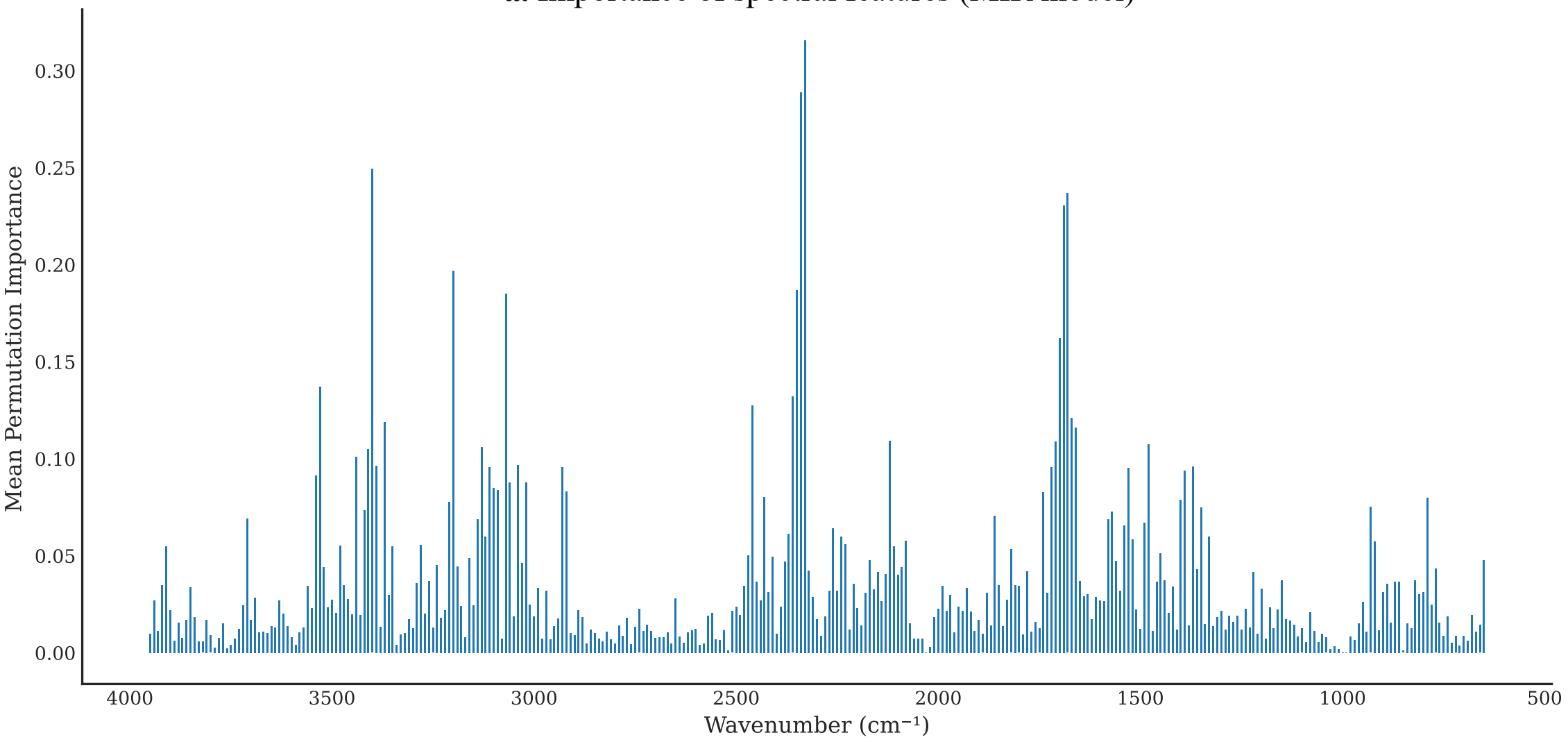

b. Importance of spectral features (VisNIR model)

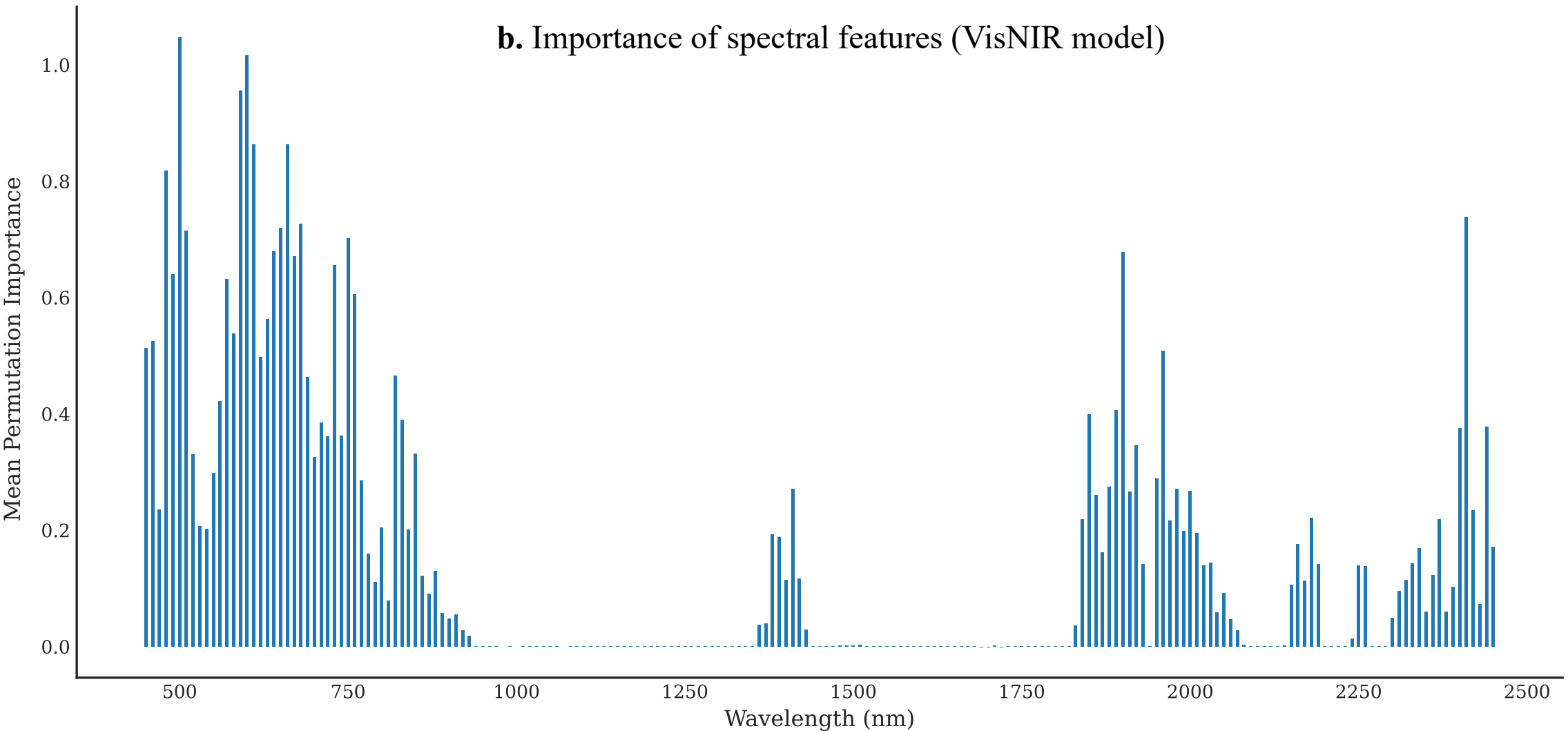

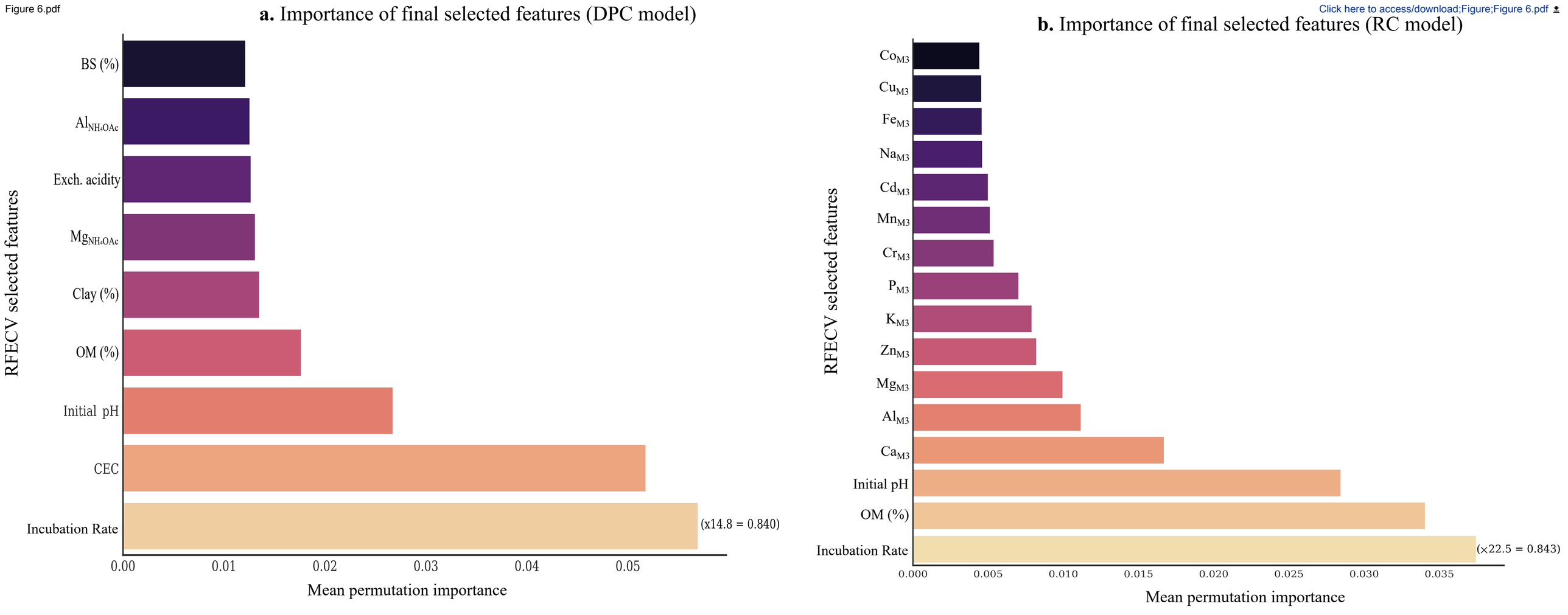

Observed ΔpH Predicted ΔpH Observed Fit Predicted Fit

a. MIR Model

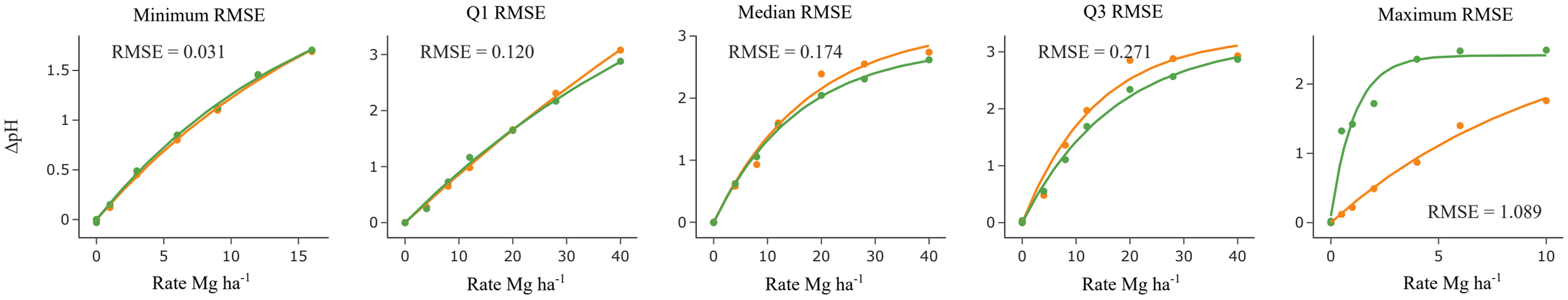

b. VisNIR Model

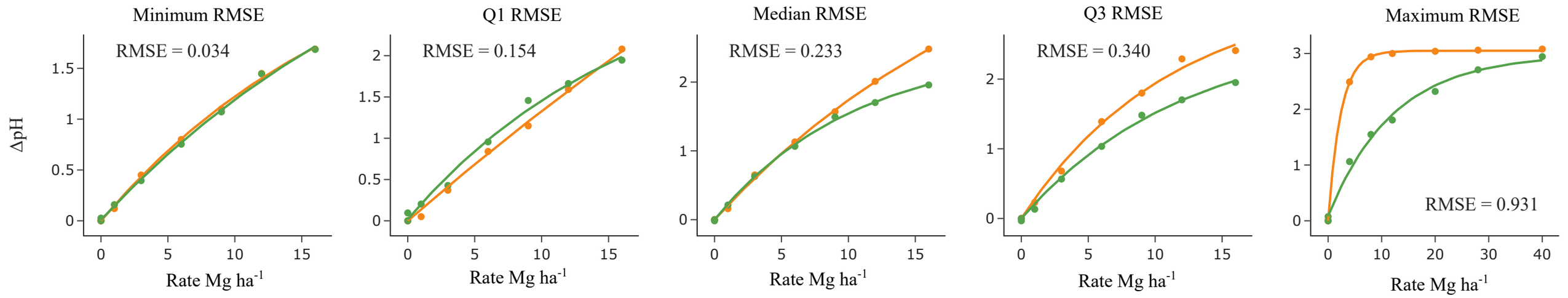

c. DPC Model

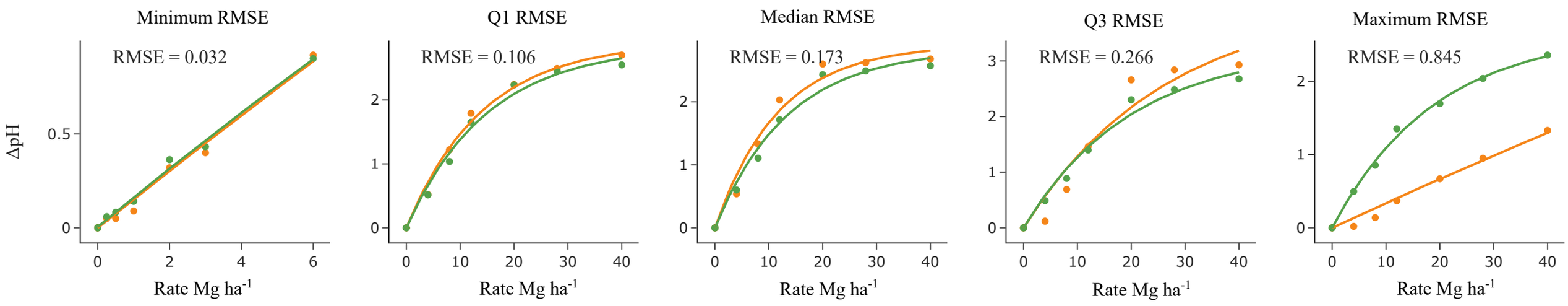

d. RC Model

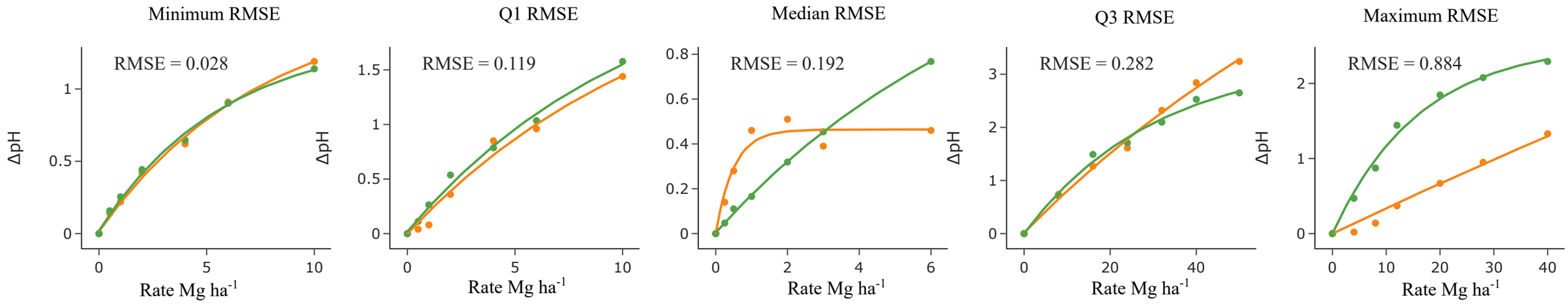

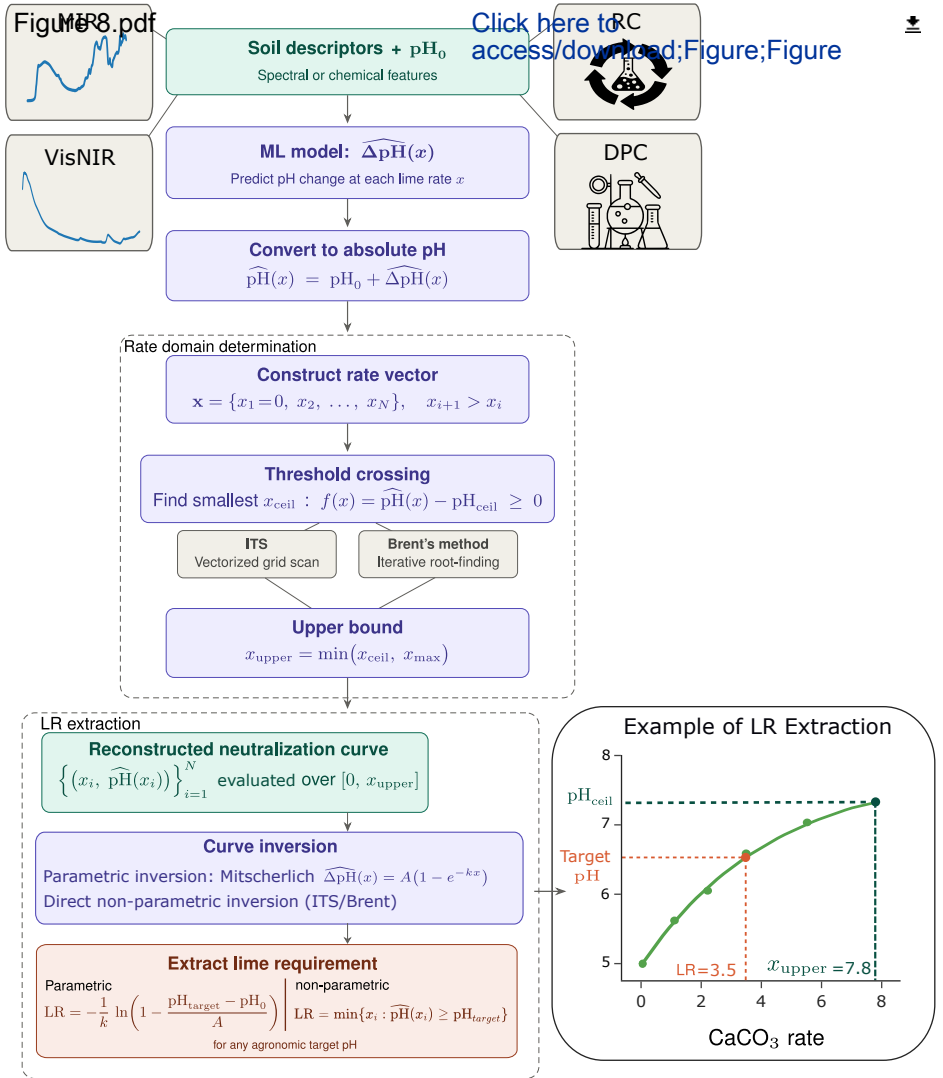

Figure 9.pdf

Click here to access/download;Figure;Figure 9.pdf

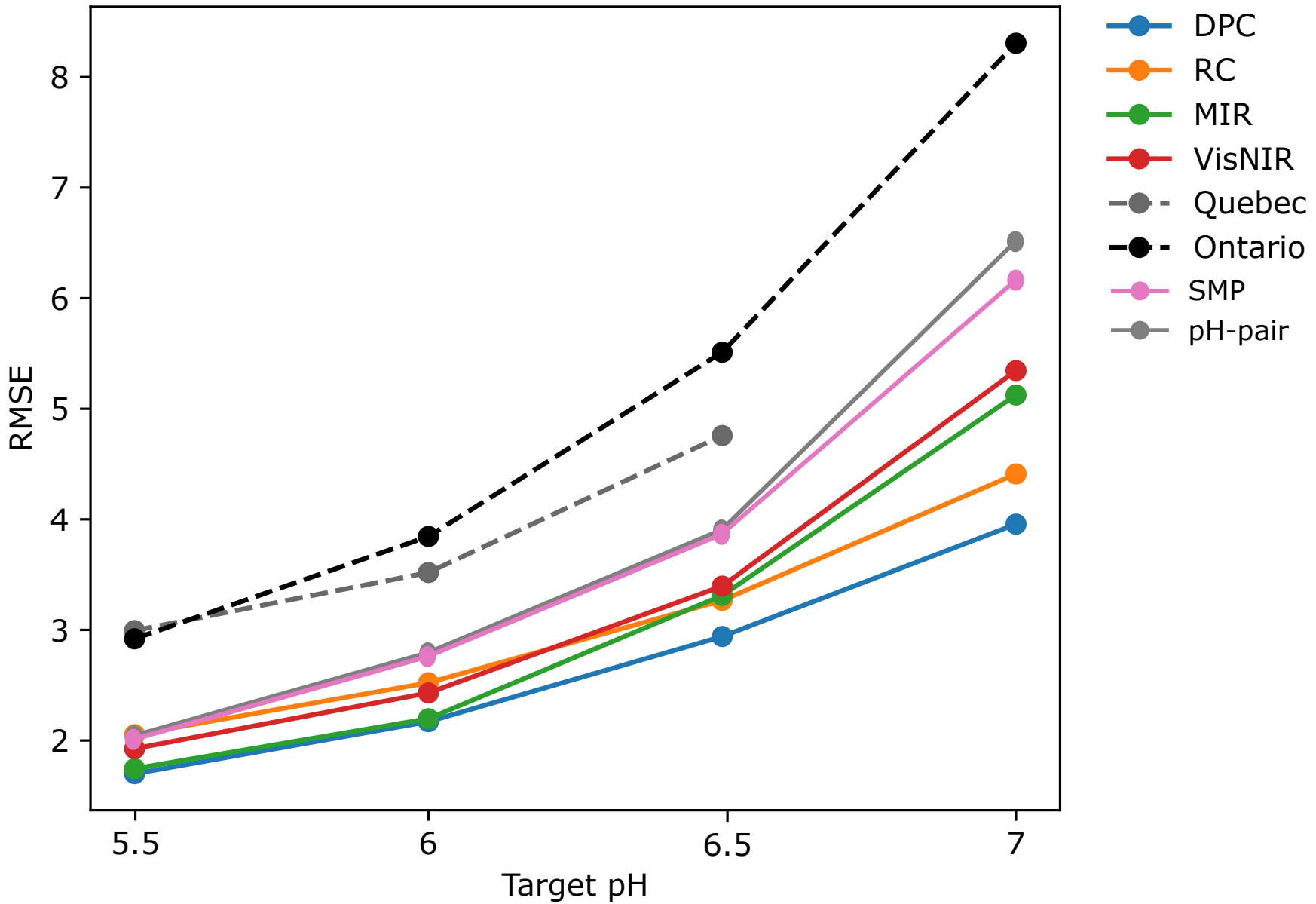

Fig. 1. Study area, sampling distribution, and North American regions historically using the SMP buffer method.
Red dots indicate the 400 soil sampling sites. Canadian provinces and U.S. states that historically reported using the Shoemaker–McLean–Pratt (SMP) buffer method are highlighted in ochre yellow. The red-dashed box outlines the main study area, and the inset provides a higher-resolution view of sampling density within this region.

Fig. 2. Raw and preprocessed MIR and VisNIR spectra of the studied soils.
(a) Raw MIR spectra; (b) raw VisNIR spectra; (c) preprocessed MIR spectra (SG1–SNV); and (d) preprocessed VisNIR spectra (SG1). Grey lines represent individual soil spectra, and the blue line represents the mean spectrum.

Fig. 3. Workflow for ΔpH prediction and neutralization-curve reconstruction.
The workflow includes spectral preprocessing, feature selection, model training, and model evaluation. Raw MIR and VisNIR spectra were first trimmed, subsampled, and preprocessed, yielding SG1–SNV for MIR and SG1 for VisNIR. Chemical and preprocessed spectral variables were then filtered for collinearity and submitted to recursive feature elimination with cross-validation (RFECV). Model development combined Bayesian hyperparameter optimization, training on 80% of the soils, unbiased testing on the remaining 20% (evaluation a), and robust 10-fold cross-validation on the full dataset (evaluation b). RF was used exclusively with chemical feature sets, whereas Cubist was used for spectral and hybrid feature sets. SG1: Savitzky–Golay first derivative; SNV: standard normal variate; RFECV: recursive feature elimination with cross-validation; RF: random forest; CV: cross-validation; MIR: mid-infrared; VisNIR: visible–near infrared.

Fig. 4. Observed versus predicted ΔpH for representative model families under 10-fold cross-validation.
Scatterplots of measured versus predicted ΔpH for (a) mid-infrared spectroscopy (MIR), (b) visible–near infrared spectroscopy (VisNIR), (c) detailed pedological characterization (DPC), and (d) routine chemistry (RC). The dashed line represents the 1:1 relationship, and the red line represents the fitted regression. Performance metrics shown in each panel correspond to the 10-fold cross-validation evaluation. R^2: coefficient of determination; RMSE: root mean squared error; RPIQ: ratio of performance to interquartile distance.

Fig. 5. Permutation importance of spectral features for ΔpH prediction.
Mean permutation importance values across spectral variables for (a) the mid-infrared (MIR) model and (b) the visible–near infrared (VisNIR) model. Higher values indicate spectral regions contributing more strongly to ΔpH prediction.

Fig. 6. Permutation importance of selected predictors for ΔpH prediction.
Mean permutation importance values of RFECV-selected features for (a) the detailed pedological characterization (DPC) model and (b) the routine chemistry (RC) model under 10-fold cross-validation. Higher values indicate greater contribution of individual predictors to ΔpH prediction. RFECV: recursive feature elimination with cross-validation; CEC: cation exchange capacity; OM: organic matter; BS: base

saturation; Exch. acidity: exchangeable acidity; M_3: Mehlich-3 extractable; NH_4OAc: ammonium acetate (pH 7).

Fig. 7. Representative observed and predicted neutralization curves under 10-fold cross-validation.
Observed and predicted ΔpH responses to $CaCO_3$ application for soils corresponding to the minimum, first quartile (Q1), median, third quartile (Q3), and maximum curve-level root mean squared error (RMSE) in (a) the mid-infrared (MIR) model, (b) the visible–near infrared (VisNIR) model, (c) the detailed pedological characterization (DPC) model, and (d) the routine chemistry (RC) model. Points represent observed and predicted ΔpH values, and lines represent the corresponding fitted neutralization curves.

Fig. 8. Inference-time workflow for reconstructing soil-specific neutralization curves and deriving lime requirement.
Starting from soil descriptors and initial soil pH (pH_0), the model predicts pH gain across a range of candidate $CaCO_3$ rates. Predicted ΔpH values are converted into absolute pH to reconstruct a soil-specific pH/ $CaCO_3$ response curve, from which lime requirement (LR) is derived for any target pH through parametric or non-parametric inversion. MIR: mid-infrared spectroscopy; VisNIR: visible–near infrared spectroscopy; RC: routine chemistry; DPC: detailed pedological characterization.

Fig. 9. Root mean squared error (RMSE) of lime requirement estimates across target pH values.
Fig. 9. Root mean squared error (RMSE) of lime requirement estimates across target pH values. RMSE between incubation-derived lime requirement and estimates obtained from machine-learning models based on detailed pedological characterization (DPC), routine chemistry (RC), mid-infrared spectroscopy (MIR), and visible–near infrared spectroscopy (VisNIR), as well as from reduced potentiometric models (SMP and dual-pH) and regional SMP table-based recommendations for Québec and Ontario, evaluated at target pH values of 5.5, 6.0, 6.5, and 7.0. SMP: Shoemaker–McLean–Pratt buffer pH; dual-pH: model using both pH_{water} and pH_{SMP} as input variables.

Declaration of interests

☒The authors declare that they have no known competing financial interests or personal relationships that could have appeared to influence the work reported in this paper.

☐The authors declare the following financial interests/personal relationships which may be considered as potential competing interests: